Taylor & Francis
Taylor & Francis Group



Expert Opinion on Drug Discovery

ISSN: 1746-0441 (Print) 1746-045X (Online) Journal homepage: www.tandfonline.com/journals/iedc20

# Nano differential scanning fluorimetry in drug discovery: advances, applications, and limitations

Atilio Reyes Romero , Alexander S. S. Dömling & Matthew R. Groves

**To cite this article:** Atilio Reyes Romero , Alexander S. S. Dömling & Matthew R. Groves (02 Nov 2026): Nano differential scanning fluorimetry in drug discovery: advances, applications, and limitations, Expert Opinion on Drug Discovery, DOI: 10.1080/17460441.2026.2757577

**To link to this article:** https://doi.org/10.1080/17460441.2026.2757577

© 2026 The Author(s). Published by Informa UK Limited, trading as Taylor & Francis Group.

Published online: 02 Nov 2026.

Submit your article to this journal

View related articles

View Crossmark data

Full Terms & Conditions of access and use can be found at
https://www.tandfonline.com/action/journalInformation?journalCode=iedc20

EXPERT OPINION ON DRUG DISCOVERY
https://doi.org/10.1080/17460441.2026.2757577

Taylor & Francis
by informa

REVIEW

OPEN ACCESS Check for updates

# Nano differential scanning fluorimetry in drug discovery: advances, applications, and limitations

Atilio Reyes Romero[a,b], Alexander S. S. Dömling[a,b] and Matthew R. Groves[c,d]

[a]Regional Centre of Advanced Technologies and Materials, Czech Advanced Technology and Research Institute (CATRIN), Palacký University Olomouc, Olomouc, Czech Republic; [b]Institute of Molecular and Translational Medicine, Faculty of Medicine and Dentistry, Palacký University and University Hospital Olomouc, Olomouc, Czech Republic; [c]Faculty of Science and Engineering, Chemical and Pharmaceutical Biology - Groningen Research Institute of Pharmacy, University of Groningen, Groningen, The Netherlands; [d]Genomics for Health in Africa (GHA), Africa-Europe Cluster of Research Excellence (CoRE)

**ABSTRACT**

**Introduction:** Nano differential scanning fluorimetry monitors changes in the intrinsic tryptophan and tyrosine fluorescence of a target protein during thermal unfolding, providing a label-free approach to assessing protein stability and ligand engagement in early-stage drug discovery.

**Areas covered:** The authors examine the technical differences between nano differential scanning fluorimetry and dye-based differential scanning fluorimetry, including sample demand, throughput, buffer and solvent compatibility, and optical artifacts. In addition, the authors present applications in fragment screening, hit validation, and the characterization of oligomeric, allosteric, membrane, proximity-induced degradation modalities and RNA-binding targets. Finally, the limitations arising from reporter distribution, noncooperative unfolding, aggregation, and complex matrices are highlighted. This review is based on literature searches using PubMed and Google Scholar to identify articles published between 2001 and 2026.

**Expert opinion:** NanoDSF is most valuable as a context-dependent primary or orthogonal method rather than a universal high-throughput replacement. Its future impact will depend on automation, analysis of raw fluorescence and scattering, validated reconstituted systems, and integration with quantitative binding, structural, and functional assays. Expansion to cell-like matrices will require target-specific deconvolution.

**ARTICLE HISTORY**
Received 31 August 2026
Accepted 28 October 2026

**KEYWORDS**
Drug discovery; high-throughput screening; membrane proteins; nanoDSF; target engagement; thermal shift assay

## 1. Introduction

### 1.1. Challenges in early-stage drug discovery

Certain classes of targets are widely regarded as 'undruggable,' as they are refractory to modulation by conventional small molecules that rely on deep anchorage within hydrophobic binding pockets [1–3]. Protein-protein interaction surfaces exemplify this category, since they are often large and relatively flat, with binding energy concentrated in discrete hotspots and fewer preformed pockets than conventional enzyme active sites. Nevertheless, their involvement in numerous pathologies, including cancer, makes them highly attractive therapeutic targets [4]. Other historically intractable targets include intrinsically disordered oncoproteins such as MYC [5], and highly conserved small guanosine triphosphatases (GTPases) such as RAS, with KRAS representing the most frequently mutated oncogene across human cancers [6]. In the latter case, the primary challenge lies in the extreme conservation of the nucleotide binding pocket across the approximately 150–200 small GTPases encoded by the human genome (e.g. Ras, Rho, Rab, and Arf families), as well as the Gα subunits of heterotrimeric G proteins, leaving little structural basis for selective targeting [7]. Contemporary biophysical approaches are therefore required not only to sustain sufficient throughput for large compound collections, but also, and more critically, to deliver high signal-to-noise ratios and the sensitivity to detect minor perturbations, like in the cases of low-affinity binding events [8]. High-throughput assays provide broad coverage of chemical space but remain susceptible to artifacts arising from nonspecific binding, compound aggregation, surface adsorption and target instability. Well-established methodologies such as nuclear magnetic resonance (NMR), surface plasmon resonance (SPR) and isothermal titration calorimetry (ITC) confirm target engagement with greater confidence yet are less scalable and considerably more sample-demanding, thus leaving a methodological gap for low-volume, label-free assays in early-stage drug discovery.

### 1.2. Literature search methodology

PubMed and Google Scholar were searched for publications from 2001 to 2026. Search terms included 'nano differential scanning fluorimetry,' 'intrinsic fluorescence,' 'differential scanning fluorimetry' and 'thermal shift assay,' combined with terms related to drug discovery, fragment screening, membrane proteins, biologics, protein-RNA interactions, antibodies,

**CONTACT** Matthew R. Groves m.r.groves@rug.nl Department of Chemical and Pharmaceutical Biology, University of Groningen, Groningen 9713 AV, The Netherlands

© 2026 The Author(s). Published by Informa UK Limited, trading as Taylor & Francis Group.
This is an Open Access article distributed under the terms of the Creative Commons Attribution-NonCommercial-NoDerivatives License (http://creativecommons.org/licenses/by-nc-nd/4.0/), which permits non-commercial re-use, distribution, and reproduction in any medium, provided the original work is properly cited, and is not altered, transformed, or built upon in any way. The terms on which this article has been published allow the posting of the Accepted Manuscript in a repository by the author(s) or with their consent.

**Article highlights**

- Provides a current review of the use of nanoDSF in drug discovery programs. It focuses on recent developments and highlights both successful use cases and limitations in data acquisition or analysis.

aggregation and targeted protein degradation. Additional studies were identified from the reference lists of relevant publications. Primary research and methodological studies were prioritized according to their relevance to assay performance, experimental limitations and applications in drug discovery. Full texts and supplementary materials were examined to verify assay formats, experimental conditions and the interpretation of thermal responses.

### 1.3. Evolution from dye-based DSF to nanoDSF

Differential scanning fluorimetry (DSF), introduced as the ThermoFluor platform in the late 1990s [9] became broadly accessible once SYPRO Orange was shown to be compatible with the optical filters of real-time polymerase chain reaction (PCR) thermocyclers [10,11] and was rapidly adopted for the systematic optimization of salts, pH, reducing agents and additives to improve protein solubility and crystallizability [12–14]. It was also established as an *in vitro* target-engagement method: Niesen et al. described a rapid screen for low molecular weight ligands that bind and stabilize purified proteins [11]. Subsequently, in 2013, the group of Professor Pär Nordlund at the Karolinska Institutet transformed the field by introducing the cellular thermal shift assay (CETSA), which enabled drug target engagement to be assessed directly in intact cells by measuring protein thermal stability within a native cellular environment [15,16]. However, this approach remained dependent on a detection marker. The real technological leap occurred in approximately the same period, between 2012 and 2014, when NanoTemper Technologies introduced the nano differential scanning fluorimetry (nanoDSF). The key innovation of this method was the complete elimination of any external chemical dye, instead relying on native fluorophores already present in the sample.

### 1.4. Principle of nanoDSF

NanoDSF monitors intrinsic tryptophan (Trp) and, less strongly, tyrosine (Tyr) fluorescence. We use the established term nanoDSF to denote intrinsic-fluorescence differential scanning fluorimetry; the prefix does not refer to nanolitre sample volumes or to a particular protein concentration. Thermal unfolding changes residue polarity and the solvent accessible surface area, altering emission at 330 and 350 nm. Fluorescence emission at 330 nm (F330) and 350 nm (F350) is recorded, and the temperature-dependent F350/F330 ratio is commonly used to identify transitions. Removing the external dye reduces handling and reporter-related artifacts, but an informative response still requires that unfolding or ligand binding alter the environment of one or more aromatic reporters.

## 2. Technical and methodological advances

### 2.1. Dye-dependent and dye-free detection

While DSF detects protein unfolding with an extrinsic reporter, dye-free assays instead monitor the environment-sensitive fluorescence of intrinsic tryptophan and, less strongly, tyrosine. A schematic comparison of the operating principles of the two techniques is provided in Figure 1.

The most widely used dye in conventional DSF is SYPRO Orange, whose fluorescence is strongly quenched in aqueous solution but increases when the dye binds the hydrophobic patches of the protein progressively exposed during thermal unfolding [17]. A typical DSF fluorescence profile and its first derivative, used to identify an apparent melting temperature ($T_m$), are shown in Figure 2(A,B). SYPRO Orange is compatible with standard PCR optical modules because it can be excited in the blue region, around 470–490 nm, and emits in the orange-red region, around 570–580 nm. This spectral profile, together with its high signal-to-background ratio and use at low final concentrations, typically 1–5× from a commercial 5000× stock in 100% dimethyl sulfoxide (DMSO), makes it highly practical for medium- and high-throughput thermal shift screening, with typical assay volumes ranging from 10 µL in 384-well plates to 50 µL in 96-well plates. However, compounds that absorb or emit within the SYPRO Orange detection window can interfere with the readout, producing apparent stabilization or destabilization that does not reflect target engagement, although this risk is lower than with dyes excited in the near-ultraviolet (UV), such as 1-anilinonaphthalene-8-sulfonic acid (1,8-ANS) [20].

The dye itself binds the hydrophobic regions exposed during unfolding, which are also the surfaces available to ligands, cofactors, additives, or excipients [11]. This is a direct consequence of the detection principle: SYPRO Orange reports on surface hydrophobicity, and its emission depends on the polarity of its local environment and on its contacts with the protein [21]. A small molecule occupying an exposed apolar cavity therefore binds the same surfaces that generate the signal and may do so with higher affinity than the dye. This is particularly problematic when screening hydrophobic drug candidates, poorly soluble fragments, aggregators, and pan-assay interference compounds [22], or formulation excipients that can sequester the dye. Furthermore, binding of the dye to a compound or to a solvent component raises the pre-transition fluorescence and reduces the amplitude of the unfolding transition [11]. In such cases, a true binder may appear inactive because it prevents dye access, reduces the unfolding-associated fluorescence increase, or modifies the shape of the melting curve. Since the magnitude of a thermal shift also depends on the unfolding energetics of the protein and on the stoichiometry of the interaction, a reduced or distorted signal does not by itself indicate absence of binding [23]. Conversely, a non-binder may appear as a false hit if it interacts directly with the dye, alters dye quantum yield, or contributes its own fluorescence to the signal. Protein-independent fluorescence can also originate from nominally inert buffer

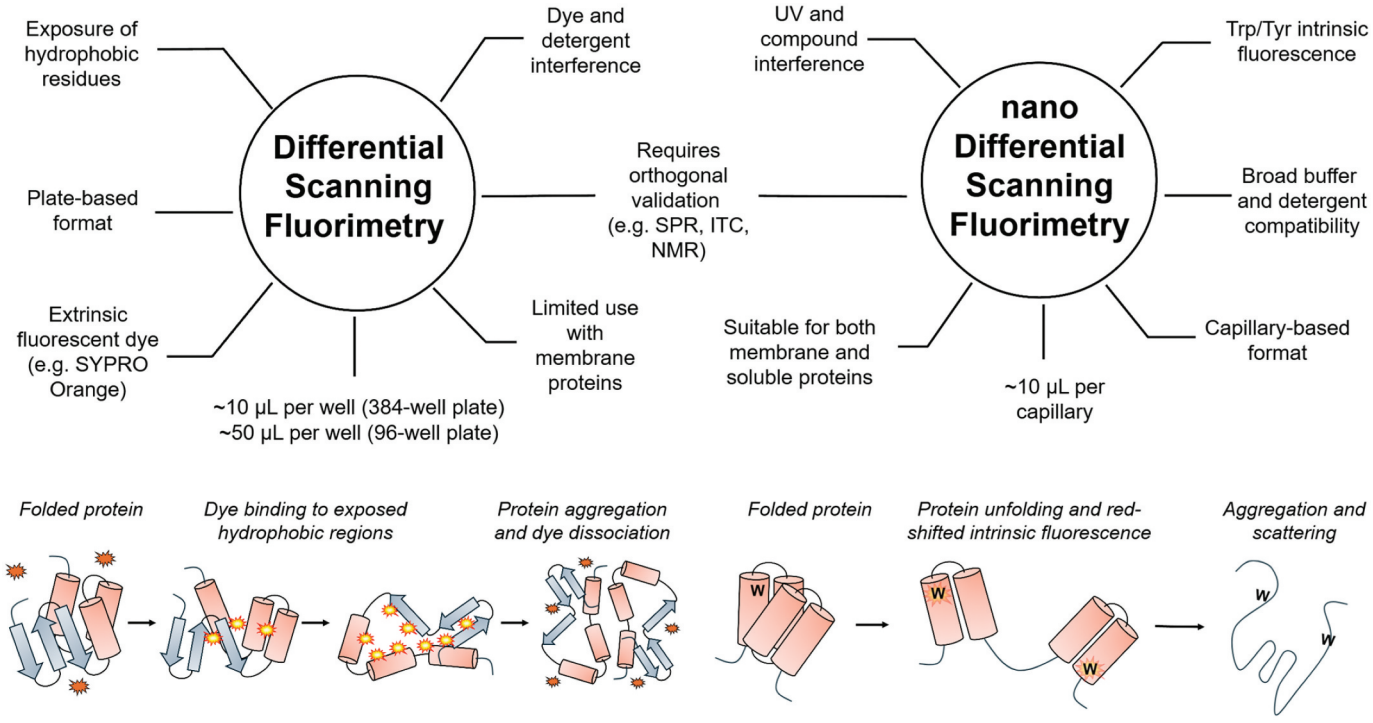



Figure 1. Comparison of conventional dye-based differential scanning fluorimetry and nano differential scanning fluorimetry. Schematics are not to scale. Simplified operating principles and fluorescence readouts of the two techniques during a temperature ramp are shown. The two instrument schematics were developed with ChatGPT (OpenAI; GPT-6.1 Sol) from the authors' concepts and specifications.

components: concentrated ethylenediaminetetraacetic acid, for example, forms pH-dependent aggregates that activate SYPRO Orange [24]. These reporter-related effects require dye-only controls and, where available, dye-free counter-screens to distinguish a protein-dependent response from an artifact of detection.

A further limitation of SYPRO Orange is its incompatibility with many detergent-containing formulations, which is particularly relevant for membrane proteins. Membrane proteins often require amphiphilic solubilizing agents such as n-dodecyl-β-D-maltoside (DDM), n-decyl-β-D-maltoside, lauryl maltose neopentyl glycol (LMNG), and 3-[(3-cholamidopropyl) dimethylammonio]-1-propanesulfonate. These additives provide hydrophobic micellar or lipid-like environments that can bind hydrophobic dyes directly, producing high background fluorescence, abnormal melting profiles, reduced dynamic range, or complete loss of a usable transition. Alternative dye-based approaches, including thiol-reactive maleimide assays, can be applied to detergent-solubilized membrane proteins, with the constraints discussed in Section 4.1 [25]. More recent protein-adaptive DSF approaches use panels of conformationally responsive dyes to select a suitable reporter for each target, thereby recovering interpretable transitions that may be missed with SYPRO Orange alone [26].

NanoDSF removes the added environment-sensitive reporter and follows intrinsic tryptophan and tyrosine fluorescence. Figure 2(C–E) presents experimental examples of nanoDSF raw-fluorescence, ratio and first-derivative readouts for pleconaril-stabilized human rhinovirus A2 (RV-A2) [18]. Ligand-dependent back-reflection scattering of DtpB and the corresponding DtpB–L-Ala–L-Pro–L-Phe (APF) structure are shown in Figure 2(F,G) [19]. Unlike SYPRO Orange DSF, nanoDSF adds no reporter that can interact with compounds, detergents or buffer components, and, unlike thiol-reactive maleimide assays, it requires no covalent derivatization of cysteine residues. However, dye-free should not be interpreted as interference-free. Compounds absorbing near the excitation wavelength can reduce the light reaching protein fluorophores through a primary inner-filter effect, lowering fluorescence intensity and potentially compromising the signal-to-noise ratio. Absorption at the emission wavelengths produces a secondary inner-filter effect through reabsorption of emitted light; when attenuation differs between 330 and 350 nm, the F350/F330 baseline can shift or the transition can be distorted [27]. Compound fluorescence can also increase the initial signal and obscure the protein response. The F350/F330 ratio compensates for attenuation shared by both channels when sufficient signal remains, but it cannot correct additional compound fluorescence or unequal attenuation of the two emissions. Such interference need not produce a measurable shift in apparent $T_m$ and may therefore escape detection if only melting temperatures are inspected. These problems deserve particular attention in libraries rich in aromatic and heteroaromatic scaffolds, whose ultraviolet absorbance overlaps both the 280 nm excitation and the 330–350 nm emission windows of intrinsic fluorescence. The 470–490 nm excitation and 570–580 nm emission of SYPRO Orange lie largely outside this range.

In summary, all DSF formats are sensitive to the fluorescence properties of library components, which can broaden the background of thermal profiles and generate false negatives. Extrinsic dyes alleviate this to some extent by amplifying

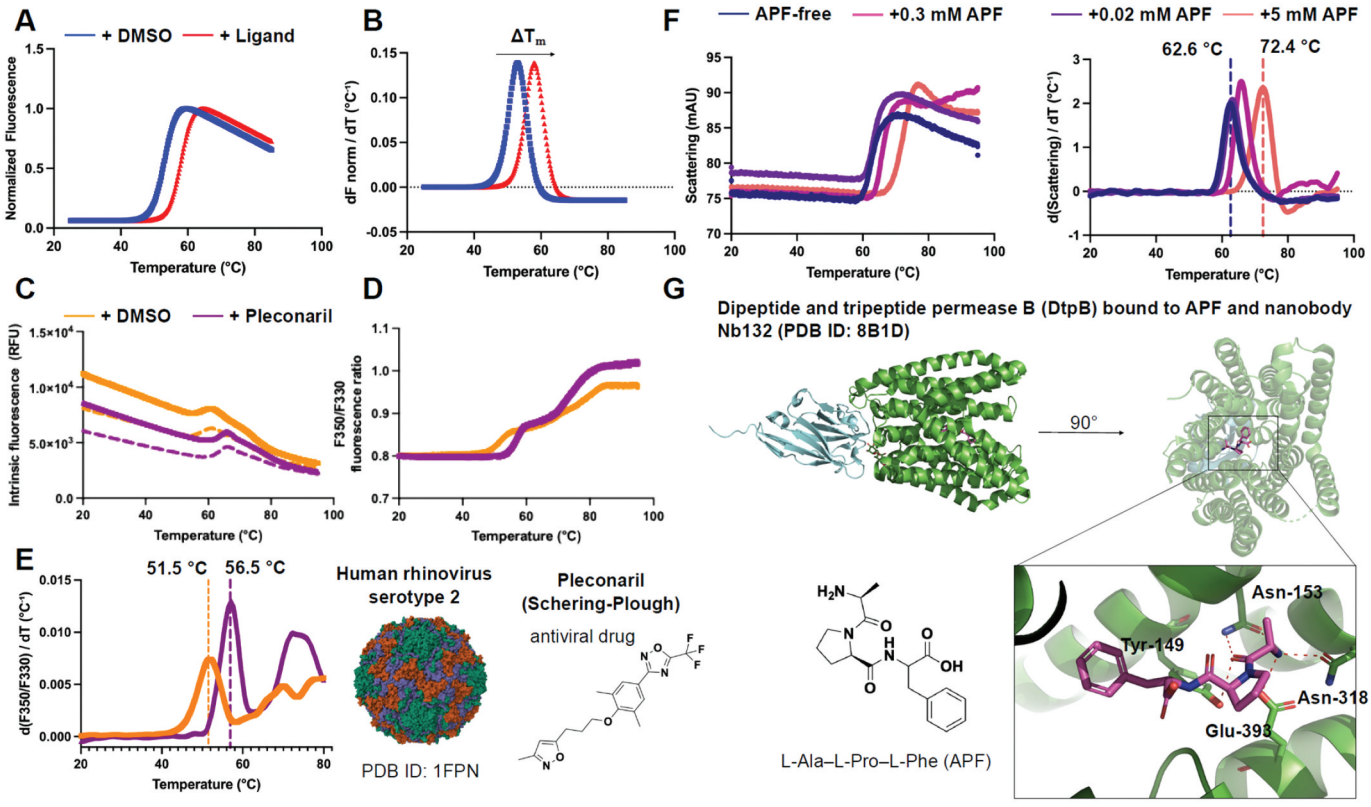



Figure 2. Comparison of simulated dye-based DSF profiles and experimental nanoDSF readouts for resolving ligand-induced stabilization, structural rearrangements and aggregation. Conventional dye-based DSF profiles showing normalized dye fluorescence (A) and its first derivative (B), illustrating the determination of an apparent ligand-induced thermal shift. (C–E) Representative experimental nanoDSF readouts obtained during the heat-induced capsid rearrangement of human rhinovirus A2 (RV-A2) in the presence of DMSO (orange) or 1 mM pleconaril (purple). The raw intrinsic fluorescence signals recorded at 330 and 350 nm are shown as solid and dashed lines, respectively. The corresponding F350/F330 fluorescence ratio (D) and its first derivative (E) reveal pleconaril-mediated stabilization of the native capsid, shifting its transition into the A-particle state from 51.5 to 56.5°C. The native RV-A2 capsid and the chemical structure of pleconaril are shown alongside the profiles (Protein Data Bank (PDB) ID: 1FPN). (F) Back-reflection scattering profiles of the peptide transporter DtpB in the absence or presence of increasing concentrations of the tripeptide substrate L-Ala–L-Pro–L-Phe (APF). The profiles illustrate ligand-dependent changes in particle scattering consistent with changes in conformational or oligomeric state. (G) Structure of the DtpB–APF complex stabilized by nanobody Nb132 (PDB: 8B1D). DtpB and Nb132 are shown as green and cyan ribbon representations, respectively, whereas APF is shown as magenta sticks. The enlarged binding pocket shows APF and selected DtpB residues in stick representation, with polar contacts indicated by red dashed lines. Panels A and B were generated for this review. Panels C–E were adapted from Real-Hohn et al. under CC BY 4.0 [18]. Panel F was replotted from the numerical dataset deposited by Kotov et al. [19] under CC BY 4.0, with the authors' permission; these scattering traces were not shown in the published article. Panel G was prepared from PDB entry 8B1D.

the unfolding signal, although screening components may still interact with the reporter [20]. The practical impact depends on compound concentration, spectral overlap, optical path length and fluorescence collection geometry. Where interference is confirmed, dye-based DSF offers the option of selecting a reporter with a different spectral window, and systematic dye libraries now make this practical [26], an option unavailable when the fluorophore is the protein itself.

### 2.2. Sample efficiency and throughput

Generally, nanoDSF combines low sample demand with parallel acquisition, although its throughput profile differs from that of plate-based formats. The Prometheus NT.48 measures 48 capillaries per run at a 10 µL loading volume, and High Sensitivity capillaries allow measurement at lower protein concentrations [28]. In the enzyme-library workflow of Magnusson et al., this corresponded to less than 10 µg of protein per measurement [29]. Working with hypotonic extracts and single measurements, the authors reported 288 melting-temperature determinations per day and processed 552 unknown variants over two working days. Fragment screening reaches a comparable rate. Screening the 768-member Diamond–SGC–iNEXT Poised (DSi-Poised) library on a 48-capillary Prometheus NT.48 required 16 runs of approximately 1.5 h each, allowing four to six plates per working day and completion of the library in three to four days [28]. Throughput is therefore governed by run duration rather than by sample preparation, and automated loading reduces hands-on time without altering this constraint. Both figures remain below what dye-based DSF achieves in automated 384-well plates [30]. Assay choice must follow library size, target behavior, and the relative risks of dye-related and intrinsic-fluorescence interference.

### 2.3. Buffer, solvent and matrix compatibility

Removing the dye broadens the range of buffers and additives that nanoDSF can test, but buffer composition and other sample components can still affect protein stability and the optical readout. Reducing agents, pH, ionic strength, excipients, cosolvents, and amphiphiles all affect both protein

thermodynamics and the optical baseline. The practical advantage is that these effects can be compared without the added variable of interactions between the dye and buffer additives, provided each matrix is tested with matched blanks, identical solvent content, and inspection of the raw F330, F350, and scattering traces. The MoltenProt workflows have been used this way to rank buffer conditions and compare protein complexes and membrane-protein preparations, and the authors show that parameters beyond $T_m$ may be needed when unfolding is non-two-state [31]. Compatibility with crude or solvent-rich samples depends on conditions that must be verified for each target. For example, the enzyme-library workflow described above screened six enzymes against eight water-miscible cosolvents, all of which produced concentration-dependent destabilization. Reliable measurement depended on the target contributing sufficient intrinsic fluorescence relative to that of other proteins in the sample. This result does not establish that nanoDSF can selectively monitor a target in an arbitrary lysate or in intact cells [29].

Published fragment workflows likewise operate at low final DMSO concentrations rather than the high levels sometimes assumed: in the 768-member DSi-Poised library screen, 100 mM stocks in 20% (v/v) DMSO were dispensed at 0.3 µL into 14.7 µL of protein, giving approximately 0.4% final DMSO, and the authors recommended establishing the DMSO tolerance of each new target [28]. Solvent-only controls must match the composition of the test samples. Because precipitation can mimic a binding response, an apparent shift that grows with compound concentration has to be interpreted alongside capillary appearance and scattering. Detergent micelles are one of the clearest areas in which intrinsic-fluorescence nanoDSF expands practical assay space where dye-based DSF performs poorly. Kotov et al. screened nine integral membrane proteins across 94 detergents, combining F350/F330 unfolding profiles with static light scattering. LMNG stabilized all five transporters analyzed, whereas several fos-choline and polyethylene glycol detergents produced soluble but already unfolded or strongly destabilized protein; detergent-only fluorescence or high scattering rendered some conditions unusable altogether [32]. NanoDSF can therefore guide detergent selection, provided each condition is shown to be interpretable: removing the dye removes dye–micelle binding, not detergent fluorescence or scattering.

### 2.4. Integration with complementary technologies

Bruch et al. integrated nanoDSF, cryogenic electron microscopy, size-exclusion ultra-performance liquid chromatography, SPR, and hydrogen-deuterium exchange mass spectrometry to rationalize the broader cross-neutralizing capacity of a booster vaccine based on the Beta variant of the severe acute respiratory syndrome coronavirus 2 (SARS-CoV-2) spike protein [33]. For both ancestral and Beta trimers, nanoDSF showed that the first thermal transition occurred at a lower temperature in cold-stored material than in material incubated at 37°C, indicating lower conformational stability. Aggregation generally followed the same trend, except for the ancestral trimer, for which the cold-stored sample showed a higher aggregation temperature. Size-exclusion ultra-performance liquid chromatography showed that the trimeric state was preserved in both conditions, with no detectable monomeric species or degradation fragments. The 37°-C-treated samples nonetheless eluted later than their cold-stored counterparts: 32.54 versus 32.07 min for the Beta spike, and 31.51 versus 30.70 min for the ancestral spike. Later elution is consistent with a less extended population, and the peaks were also narrower and more symmetrical, indicating greater conformational homogeneity. Cryo-EM showed the same distinction directly at the structural level, with incubation at 37°C restoring canonical trimers. The restored trimers differed between strains, the ancestral protein adopting a conformation with one receptor-binding domain (RBD) up and the Beta protein predominantly displaying two RBDs up, a difference relevant to the broader cross-neutralizing capacity of the Beta-based booster. Because all three methods converged on the same distinction, the nanoDSF signal reflected not only the generic thermal stability but also the equilibrium between distinct, co-existing conformational states in solution.

## 3. Applications in target engagement and hit validation

### 3.1. High-throughput screening and fragment-based drug discovery

In drug discovery, $\Delta T_m$ denotes the ligand-induced change in apparent melting temperature, measured in the presence of a ligand relative to a ligand-free control. For reversible unfolding at equilibrium, binding exclusively to the native state increases the apparent $T_m$. If the ligand also binds the unfolded state, the shift depends on the relative effects of binding on the two populations at the transition temperature, and thermodynamic models that include both states can predict either stabilization or destabilization [34,35]. The balance is not set by affinity alone: a single high-affinity, enthalpically driven native site can be offset by several weaker, entropically driven sites in the unfolded ensemble, so that a protein may be destabilized even while the ligand binds its native state [34]. When unfolded-state binding is negligible, the model reduces to the native-state description of Matulis et al. [36]. In experimental thermal scans, however, kinetics and irreversible aggregation may also affect the apparent transition (Section 5.3), while optical interference can complicate its detection. A negative $\Delta T_m$ should therefore not be interpreted as evidence of unfolded-state binding, and neither the sign nor the magnitude of the shift alone establishes the binding mechanism or affinity. Accordingly, $\Delta T_m$ should identify provisional thermal hits for independent binding confirmation, rather than rank compounds by affinity, which can be measured by ITC, SPR, microscale thermophoresis (MST) and NMR, or estimated from thermal data using the explicit models discussed in Section 3. This distinction is particularly important when ligands engage different sites or domains, because their effects on unfolding are not directly comparable.

Fragment-based drug discovery (FBDD) uses small molecules, often below 300 Da, to sample broad chemical space with compact libraries and high ligand efficiency [37–39].

Fragments can access challenging or traditionally 'undruggable' targets by mapping shallow binding grooves on protein surfaces that are often inaccessible to larger molecules. For focused and fragment libraries, we recommend nanoDSF as a primary biophysical screen when the target produces reproducible, interpretable thermal transitions and compounds are optically compatible at the screening concentration. Thermal hits should meet the criteria described in Section 3.

The work of Ahmad et al. on the DSi-Poised library, mentioned above, exemplifies a direct nanoDSF application in FBDD: nanolitre dispensing was combined with intrinsic fluorescence and scattering on a Prometheus NT.48, and the capillary format required 16 runs [28]. This represents a focused or medium-throughput biophysical screen rather than plate-scale high-throughput screening (HTS). In that screen, fragments were tested at approximately 2 mM, and some compounds produced fluorescence exceeding the detector's saturation limit, preventing reliable analysis even at low excitation power [28]. Reducing fragment concentration may alleviate interference but can also reduce sensitivity to weak binders. Profiles that remain uninterpretable should therefore be recorded as unassessable and retested after assay optimization or with another method that does not rely on fluorescence, rather than classified as non-binders. Optical compatibility of the target, buffer and compounds must therefore be established before screening. Figure 3(A) incorporates this assay-selection step before thermal-hit identification, curve quality control and orthogonal validation, and Figure 3 (B) shows the screening distribution and DMSO reproducibility control [28].

A smaller-scale workflow was reported by Thabault et al., who used intrinsic-fluorescence thermal profiling on a Tycho NT.6 as the first experimental filter for 29 virtually preselected compounds against lactate dehydrogenase (LDH), with MST and NMR confirming the selected hits (Section 3.5.1) [41].

The complementary case study involving dual-specificity tyrosine-phosphorylation-regulated kinase 1A (DYRK1A) is shown in Figure 3(C–E): concentration-dependent nanoDSF shifts induced by abemaciclib were followed by SPR and crystallographic confirmation of binding [40].

Dye-based DSF, by contrast, scales more readily. Gao et al. used an Echo 555 to eject 2.5 nL droplets of multicomponent reaction (MCR) reagents and assemble a plate-formatted

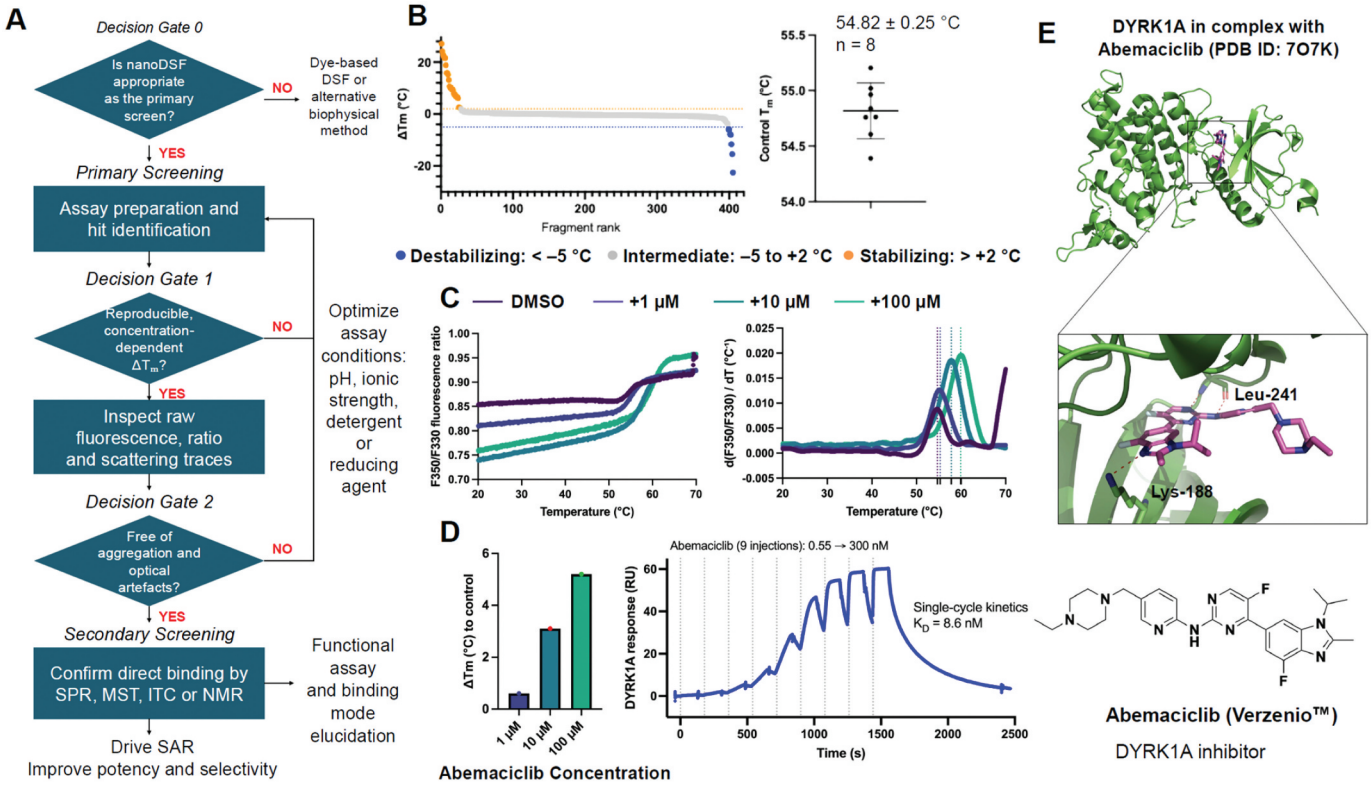



Figure 3. Examples of nanoDSF applications in drug discovery. (A) Proposed decision sequence for nanoDSF in fragment-based drug discovery. The entry gate states when nanoDSF is recommended as the primary screen rather than an orthogonal method while subsequent gates confirm reproducible, concentration-dependent $\Delta T_m$ values and reject aggregation and optical artifacts before direct-binding and functional validation. (B) Distribution of fragment-induced $\Delta T_m$ values from the DSi-Poised fragment-library screen reported by Ahmad et al., classifying fragments as stabilizing (>+2 °C), intermediate (–5 to +2 °C) or destabilizing (<–5 °C). Replicate measurements of the DMSO control provide an internal assessment of assay reproducibility. (C, D) Complementary application of nanoDSF and SPR for inhibitor prioritization and validation. Concentration-dependent changes in the F350/F330 fluorescence ratio and its first derivative (C) were observed with 1, 10 and 100 µM abemaciclib, an approved inhibitor of cyclin-dependent kinases 4 and 6 that also potently inhibits DYRK1A, producing corresponding concentration-dependent $\Delta T_m$ values (D, left). SPR single-cycle kinetics independently confirmed direct binding to DYRK1A with a $K_D$ of 8.6 nM (D, right). (E) Crystal structure of the DYRK1A–abemaciclib complex (PDB: 7O7K). DYRK1A is shown as a green ribbon representation and abemaciclib as magenta sticks, with heteroatoms colored by element. The enlarged binding pocket shows selected residues, including Lys188 and Leu241, in stick representation, with polar contacts indicated by red dashed lines. The two-dimensional chemical structure of abemaciclib is shown below the complex. Panel A presents a decision framework developed for this review. Panel B was replotted from numerical data reported by Ahmad et al., with permission from JoVE [28]. Panels C and D were replotted from data reported by Kaltheuner et al. [40] under CC BY 4.0. Panel E was prepared from PDB entry 7O7K.

library of 1,536 Groebke-Blackburn-Bienaymé three-component reaction products on a 500 nmol scale. The crude mixtures were screened against menin by conventional plate-based DSF at approximately 190 wells per hour. A positive $\Delta T_m$ cutoff of 0.5°C relative to the control was deliberately chosen to reduce false negatives among weak binders. Hits were resynthesized and purified, and subsequent MST measurements confirmed micromolar binding, including a dissociation constant ($K_D$) of 2.8 µM for I-J21, and soaking the compound into menin crystals established its binding mode. The study therefore demonstrates a direct synthesis-to-biophysics cycle in which miniaturized MCR chemistry feeds DSF at a throughput the capillary format does not currently match, but it is not a nanoDSF experiment [42]. For libraries that exceed the practical capacity of capillary screening, we favor nanoDSF as an orthogonal follow-up assay for hits from a scalable primary screen. Dötsch et al. illustrate this role at scale: a phenotypic screen of 157,332 compounds and chemical proteomics identified epoxykynin and its target, after which nanoDSF demonstrated concentration-dependent thermal stabilization of purified soluble epoxide hydrolase [43].

### 3.2. Setting and validating the hit threshold

When $\Delta T_m$ is used as a decision criterion to separate hits from non-hits, we recommend deriving an empirical threshold from the variability of replicate controls on the same run and fixing it before screening begins, rather than adopting a conventional value a priori. Published nanoDSF studies illustrate how widely these thresholds can differ. For example, Gorny et al. considered a shift significant when it exceeded three standard deviations of the ligand-free $T_m$, corresponding to ±0.22°C for voltage-dependent anion channel 1 (VDAC1); thirteen of the seventeen candidates met this criterion, of which four were subsequently confirmed by MST [44]. Kozielski et al., in turn, applied the same rule to SARS-CoV-2 nonstructural protein 10 (nsp10) and obtained a cutoff of 1.2°C, approximately fivefold higher because the control distribution was broader [45]. Thus, the same statistical reasoning produces thresholds differing by more than fivefold, and a fixed value such as 2°C would have been inappropriate in both cases. Absolute thresholds nevertheless remain common when control variability is not characterized. For example, Santhana Kumar et al. used a cutoff of 2.0°C for the phosphotyrosine-binding domain of fibroblast growth factor receptor substrate 2, applied to shifts in either direction, while excluding a compound whose autofluorescence already exceeded that of the protein [46]. This highlights an important point: decision thresholds should only be applied after optical artifacts have been excluded. The measured parameter itself may also be chosen according to the biological function of the target. In a nanoDSF screen of 1,520 approved compounds against tubulin, Baksheeva et al. defined hits using the polymerization temperature rather than $T_m$, with weak hits classified separately between 1 and 2°C [47].

The same principles apply to plate-based assays using extrinsic dyes, where larger campaigns have made the procedure explicit. Gardell et al. screened 57,004 compounds against nicotinamide phosphoribosyltransferase using distinct criteria for primary screening and confirmation, raising the Z-score threshold from 5 to 7 for confirmation and reassessing shifts in triplicate using freshly prepared solutions from powder stocks [48]. Ronzetti et al. set the cutoff two standard deviations above the mean of the DMSO control wells, equivalent to approximately 0.7°C, yielding sixteen hits from 872 compounds [49]. Control wells should be assessed before applying any threshold, since failed plates distort the reference distribution; automated tools flag these using z-scores for control amplitudes and melting temperatures [50]. A threshold defined in this way is specific to the target, buffer and plate format and cannot be transferred between campaigns without reassessment. Exceeding it identifies a provisional thermal hit rather than a confirmed binder: among the fragments screened against nsp10 by Kozielski et al., the two that exceeded the cutoff were not those for which binding was subsequently resolved by crystallography [45].

### 3.3. Distinguishing binders from assay artifacts

Before screening, compounds should be annotated for pan-assay interference compound (PAINS) alerts, reactive motifs and similarity to known aggregators. These annotations should guide additional controls rather than automatic exclusion, since many compounds carrying PAINS alerts show no elevated assay promiscuity [51,52]. Weak fragments are often tested at concentrations that increase solubility-related artifacts. A compound may precipitate after dilution from DMSO into aqueous buffer, causing scattering and distorted fluorescence [53]. For compounds flagged as potential aggregators, particle formation should be assessed in protein-free assay buffer at the screening concentration. Detergent-based retesting requires matched controls and prior validation of detergent compatibility with the target [52]. To distinguish precipitation and optical artifacts from protein-dependent responses, compare compound-only, protein-only and protein–compound samples at matched DMSO concentrations, recording the initial fluorescence, capillary appearance and scattering of each and retesting candidate hits across compound concentrations [54]. Compound-only fluorescence reveals autofluorescence, whereas absorbance at the excitation and emission wavelengths is needed to assess the primary and secondary inner-filter effects described in Section 2.

Extended conjugation and heteroaromatic substitution warrant particular attention, but aromatic-ring count alone does not establish optical compatibility, and fluorescent by-products and degradation products in a library sample can contribute as much as the nominal compound. Recurring interference should be assessed within each chemotype using measurements at the intended screening concentration. Spectral window matters more than structure: in a profiling study of HTS libraries, more than 5% of members were brighter than 10 nM 4-methylumbelliferone, and red-shifting the detection window by as little as 100 nm toward longer wavelengths produced a marked decrease in autofluorescence

[55]. If interference is confirmed, select a validated reporter with a different spectral window, as discussed in Section 2. If no compatible reporter is available, use a method that does not rely on fluorescence. Reactive or redox-active chemotypes require dedicated counterscreens: thiol-reactivity and redox-activity assays identify compounds whose apparent effects arise from covalent modification or reactive-oxygen generation rather than binding [56]. Compound integrity over the assay timescale should be verified in parallel, for example by liquid chromatography–mass spectrometry under assay-like conditions, and selected hits retested from freshly prepared material [57]. Because aggregation, optical interference and true destabilization can all produce non-canonical profiles, hits remain provisional until orthogonal confirmation.

### 3.4. Binding thermodynamics

Interpreting a thermal shift as a dissociation constant requires an explicit model of the unfolding process. Chemical denaturation offers an alternative in which affinity is estimated at a temperature of choice: the protein is unfolded across a concentration gradient of a denaturant such as urea or guanidinium at a fixed temperature, so that the midpoint of the transition is a denaturant concentration ($C_{1/2}$) rather than a melting temperature.

Ligand binding displaces this midpoint, and fitting the ligand-induced changes in the unfolding curves to an equilibrium model yields a model-dependent $K_D$ estimate across a wide affinity range, with both $C_{1/2}$ and the *m* value describing unfolding cooperativity entering the fit [58,59]. Because the fit is performed at the chosen temperature, no extrapolation from a thermal denaturation temperature is required. This matters because ligand rankings obtained at 60°C or above need not hold at physiological temperature [59]. The approach has also been applied, label-free, to an integral membrane protein: a panel of 19 compounds was evaluated against the adenosine A2A receptor, including 13 bona fide A2A agonists or antagonists and six control compounds; the resulting affinities showed strong agreement with published SPR and radioligand-binding data, particularly for high-affinity ligands [60]. Alternatively, thermal unfolding itself can be used quantitatively by measuring $T_m$ across a ligand concentration series and fitting the $T_m$-versus-concentration relationship. Bhayani and Ballicora described such a model, based on the equilibrium between native and molten-globule states and the van 't Hoff formalism, developed for dye-based DSF [61]. NanoDSF has additionally been used to monitor chemical unfolding and refolding kinetics, extending the measurement beyond a single thermal-ramp endpoint [62]. These affinity estimates remain model dependent. Equilibrium models require reversible unfolding and adequate equilibration; models for irreversible unfolding rely on distinct kinetic assumptions [63].

### 3.5. Case studies

#### 3.5.1. Oligomeric interfaces

NanoDSF is useful for investigating ligand-binding events that induce conformational changes in proteins whose activity depends on quaternary structure, including oligomeric proteins. Oligomerisation interfaces are challenging targets owing to their broad, shallow topography in monomeric or lower-order states and their extensive burial upon oligomer assembly. Thabault et al. developed a screening cascade to identify compounds targeting the tetrameric interface of LDH. Following virtual screening of the Prestwick Drug-Fragment Library, 29 candidates were evaluated by nanoDSF against tetrameric LDH-1 and LDH-5, together with an engineered dimeric construct lacking the tetramerisation arm. An interface-binding ligand was expected to destabilize the native tetramer while stabilizing the exposed interface of the dimer. At a protein concentration of 25 µg $mL^{-1}$, nanoDSF identified eight compounds with this differential thermal profile, which combined a reduction in $\Delta T_m$ for tetrameric LDH with a neutral or stabilizing effect on the dimeric construct. Following the exclusion of three compounds with structural liabilities, the remaining five candidates were validated by MST and saturation-transfer difference NMR. This screening cascade led to the final selection of F2050 and F1787, which showed binding affinities approximately 5.5-fold and 9.6-fold lower for tetrameric LDH than for dimeric LDH, respectively, consistent with competition between the compounds and the native subunits. Additionally, both compounds reduced the thermal stability of tetrameric LDH and inhibited tetramer reassociation [41].

#### 3.5.2. Cryptic and allosteric pockets

Conformationally gated cryptic allosteric pockets present a different challenge because a binding signal alone does not establish that a ligand stabilizes a therapeutically relevant state within the conformational ensemble present in solution. Maus and colleagues examined this problem using the Zika virus nonstructural protein 2B–nonstructural protein 3 (NS2B–NS3) protease, a dynamic enzyme in which the NS2B cofactor alternates between an open arrangement and a closed, catalytically competent conformation around the NS3 protease domain [64]. Rather than treating nanoDSF as a binary binder/non-binder assay, the authors combined its thermal profiles with single-molecule Förster resonance energy transfer (smFRET), conventional DSF, and 19F-NMR spectroscopy using uniformly 5-fluorotryptophan-labeled protease. smFRET showed that the competitive active-site inhibitor $I_c$ increased the closed-state population, whereas excess allosteric inhibitor $I_a$ shifted the $I_c$-stabilized population back toward the open state. Consistent with this assignment, only $I_c$ produced a chemical-shift perturbation of the W50 resonance; this residue lies adjacent to the active site and adopts a flipped orientation in the closed conformation. In nanoDSF experiments, $I_c$ produced concentration-dependent positive thermal shifts of +0.83°C at 10 µM and +2.37°C at 100 µM relative to the apo protease; by contrast, 200 µM $I_a$ resulted in a $\Delta T_m$ of −0.68°C. The study therefore shows that nanoDSF can provide a reliable and accessible readout of which conformational ensemble in solution is responsible for ligand binding when its thermal profiles are integrated with NMR and smFRET.

## 4. Emerging frontiers: challenging biomolecules and modalities

### 4.1. Membrane proteins and G protein-coupled receptors (GPCRs)

For membrane proteins, the dye–micelle interactions described in Section 2 make reporter compatibility particularly dependent on the solubilizing environment.

The thiol-reactive probe N-[4-(7-diethylamino-4-methyl-3-coumarinyl)phenyl]maleimide avoids micelle partitioning by reporting cysteine exposure rather than hydrophobic surface [25]. Its constraints are nevertheless substantial: reducing agents must be removed, the reaction is slower at low pH and less selective above pH 8, and the transition temperatures reported do not always agree with those obtained by circular dichroism. Because the cysteines of many membrane proteins are buried within transmembrane helices, the probe may also report an incomplete or perturbed transition.

NanoDSF extends these comparisons beyond detergent selection (Section 2) to the assessment of alternative membrane mimetics. Flayhan et al. followed the first derivative of F350/F330 for the peptide transporters DtpA and PepTSt and the mechanosensitive channel T2 reconstituted in saposin lipid nanoparticles; the channel was approximately 14°C more stable in a saposin-lipid environment than when solubilized in DDM [65]. Nanodiscs were long incompatible with intrinsic-fluorescence detection because the scaffold protein contributes its own aromatic signal, a limitation recently addressed by tryptophan- and tyrosine-free scaffolds that render the disc optically silent and allow the reconstituted target to be measured directly [66]. We recommend nanoDSF as a primary method for selecting membrane-protein preparations by comparing thermal stability and aggregation across constructs, detergents and lipid mimetics. For ligand discovery, we favor its complementary use alongside binding or functional assays. Primary screening of a focused library requires separate validation of ligand-dependent thermal responses and compound optical compatibility in the chosen preparation. A complementary detergent-solubilized case is VDAC1, for which nanoDSF and MST were combined to compare 17 reported ligands and identify four reproducible chemical starting points [44].

Two cautions apply. GPCR thermostabilisation has historically relied on radioligand-retention assays rather than intrinsic fluorescence [67], and constructs trapped in one conformation may alter agonist affinity; peer-reviewed nanoDSF evidence remains limited in this field. Moreover, large stability differences between mimetics show that the environment strongly influences the transition. A $T_m$ measured in detergent is therefore a property of that preparation, not a prediction of behavior in a native membrane.

### 4.2. Biologics and antibody–drug conjugates

For biologics, thermal stability is not a reporter of ligand binding but the property of interest. Antibodies do not unfold in a single step. In nanoDSF first-derivative traces, the earliest transition is usually assigned to the second constant domain of the immunoglobulin heavy chain (CH2), the least stable domain within the fragment crystallizable (Fc) region, whereas later transitions generally arise from the fragment antigen-binding and third constant heavy-chain domain (CH3) [68]. The pattern is not fixed. In a pH screen of immunoglobulin G (IgG), two transitions were resolved only under acidic conditions and at high protein concentration, while above pH 6 the CH2 transition was no longer distinguishable [69]. The unfolding onset temperature ($T_{onset}$) marks the first detectable loss of native structure. Local unfolding can expose aggregation-prone regions well before the global transition occurs. When ranking candidates by developability, $T_{onset}$ may therefore discriminate better than the apparent $T_m$. Back-reflection recorded in the same run allows conformational and colloidal stability to be compared directly, and the two need not agree [70].

Across eight National Institute of Standards and Technology monoclonal antibody (NISTmAb) formulations, conditions associated with higher conformational stability could simultaneously produce a lower aggregation-onset temperature [71]. In the IgG study by Kim et al., apparent $T_m$ showed an overall tendency to increase with pH. Aggregation behavior, however, depended on both buffer species and protein concentration. At 1 mg/mL, no aggregation was detected in acetate at pH 4.6 or below upon heating to 95°C, whereas citrate samples aggregated throughout the tested pH range. At 100 mg/mL and pH 4.6, aggregation was also observed in acetate, although its onset temperature remained higher than in citrate (61.0 versus 52.7 °C). Dynamic and static light-scattering measurements indicated repulsive protein–protein interactions in acetate and attractive interactions in citrate. This difference was also reflected in viscosity at high concentration (15.1 versus 18.0 cP at approximately 209 mg/mL) [69]. Comparable workflows have been applied to biosimilar comparability, with trastuzumab and rituximab as case studies [72].

The distinction between conformational and colloidal stability becomes critical for antibody-drug conjugates. Beckley et al. showed that conjugation left the secondary structure of a valine-citrulline-monomethyl auristatin E conjugate essentially unchanged while rendering CH2 markedly less resistant to thermal stress, with the high-molecular-weight species formed at 40°C composed predominantly of molecules carrying six or eight drugs [73]. Kaempffe et al. refined this picture using a panel of homogeneous conjugates with a drug-to-antibody ratio of 2, in which drug load was held constant: conjugation to CH3 caused no destabilization, whereas modification of CH2 or of the light-chain C-terminus lowered $T_{m,1}$ by up to 17°C. The magnitude depended on both the conjugation site and the antibody scaffold. Notably, this thermal destabilization did not correlate with faster clearance in mice or with a greater propensity to aggregate during manufacture, though the authors note it may still flag risk for other developability attributes such as agitation or oxidative stress [74]. These measurements rapidly rank constructs, linkers and formulations with little material. NanoDSF has also been used to assess whether proteins retain conformational integrity during loading into and release from nanoparticle

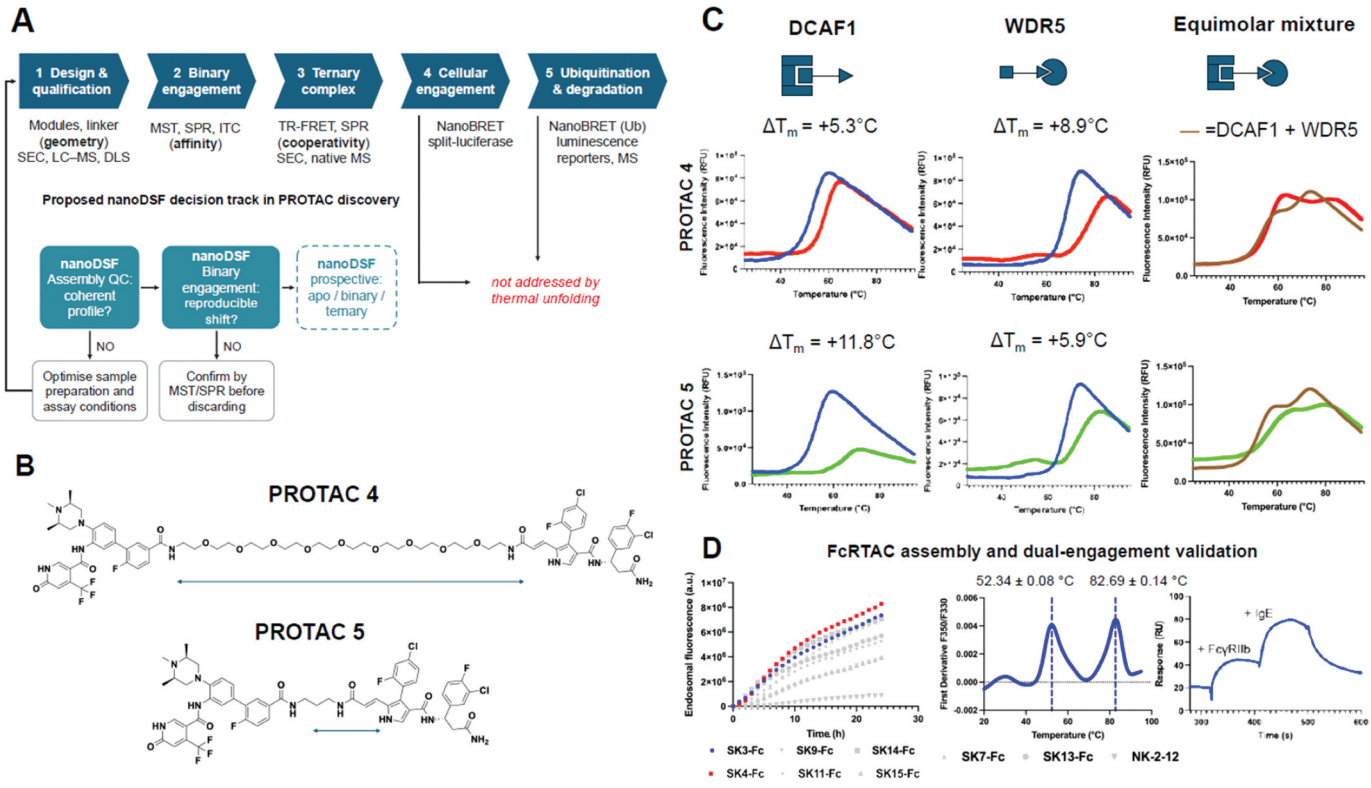



Figure 4. Applications of nanoDSF and related thermal shift approaches to targeted degradation modalities. (A) Proposed PROTAC workflow positioning nanoDSF in construct quality control and assessment of binary thermal responses alongside direct ternary-complex, cellular-engagement and degradation assays. The dashed box marks nanoDSF profiling of ternary mixtures as a prospective application. (B) Structures of DCAF1-recruiting WDR5 PROTACs 4 and 5; arrows indicate their relative linker lengths. (C) SYPRO Orange DSF showing thermal shifts for DCAF1 and WDR5 individually and fluorescence profiles of equimolar DCAF1–WDR5 mixtures without degrader (brown), with PROTAC 4 (red) or with PROTAC 5 (green). Blue color indicates individual proteins without degrader. Changes in the mixed-protein profiles provide a complementary thermal readout; ternary-complex formation was assessed independently by SPR. (D) FcRTAC development illustrated by endosomal uptake of FcγRIIb-binding single-chain variable fragment–Fc candidates, the biphasic nanoDSF profile of the assembled NK-2–12-SK3 construct and sequential SPR confirming FcγRIIb and IgE engagement. Panel A was developed for this review, while panels B and C were redrawn or adapted from Mabanglo et al. [76], with permission from Springer Nature. Panel D was replotted from Du et al. [77], with permission from the authors and Springer Nature.

formulations [75]. Thermal unfolding and aggregation measurements remain accelerated surrogates for long-term stability: they do not reliably predict aggregation during months of storage, so formulation decisions should not rest on thermal parameters alone. Beyond formulation studies, nanoDSF can also support qualification of assembled biologics. In the Fc gamma receptor IIb (FcγRIIb)-targeting chimera (FcRTAC) example, Du et al. used nanoDSF after liquid chromatography–mass spectrometry (LC–MS), before sequential SPR confirmed preserved FcγRIIb and immunoglobulin E (IgE) engagement (Figure 4(D)) [77].

### 4.3. Proximity-induced degradation modalities

Proteolysis-targeting chimeras (PROTACs) challenge the assumptions underlying conventional ligand-binding assays [78], expanding the horizon of the druggable genome [79,80]. Their pharmacological activity depends not only on the affinity of the two ligands for the protein of interest (POI) and the recruited E3 ubiquitin ligase, but also on the population, cooperativity, geometry, and lifetime of the resulting POI-PROTAC-E3 ternary complex [81]. In a systematic series of von Hippel–Lindau (VHL)-recruiting degraders of the chromatin-remodeling ATPase SMARCA2 and bromodomain-containing protein 4, ternary-complex affinity and cooperativity tracked degradation potency and initial degradation rates, whereas binary affinity did not: two degraders bound VHL approximately 7- to 9-fold more tightly than the best compound in the series, yet formed weaker ternary complexes, showed negative cooperativity, and degraded SMARCA2 inefficiently [82].

For PROTACs, dedicated ternary-complex assays are better suited than thermal unfolding to characterize recruitment of the target protein to the E3 ligase. Time-resolved Förster resonance energy transfer (TR-FRET) can monitor concentration-dependent ternary-complex formation [83], whereas SPR can quantify association and dissociation kinetics and, with matched binary measurements, cooperativity [81]. In cells, NanoLuc-based bioluminescence resonance energy transfer (NanoBRET) assays can follow target–ligase proximity, while complementary luminescence assays quantify target degradation [84]. NanoDSF has a supporting role in assessing the thermal responses of the individual protein partners. Keuler et al. examined PROTACs directed against the inflammasome sensor NLRP3, testing its nucleotide-binding NACHT domain and the recruited E3 ligases in separate samples. The control compound (–)V2 retained thermal stabilization of NLRP3 but did not stabilize VHL, providing evidence consistent with the distinct contributions of the two binding arms [85]. These experiments assessed binary interactions rather than the complete ternary complex. NanoDSF can

therefore complement direct-binding measurements and identify aggregation or atypical unfolding, but a thermal shift alone does not establish binding, ternary-complex formation or productive ubiquitination. Figure 4(A) distinguishes these complementary experimental questions.

A direct example was reported for degraders of WD repeat-containing protein 5 (WDR5) that recruit DDB1- and CUL4-associated factor 1 (DCAF1), whose chemical structures are reported in Figure 4(B). Mabanglo and colleagues used conventional DSF with SYPRO Orange as an orthogonal readout, comparing DCAF1 and WDR5 individually with equimolar DCAF1–WDR5–PROTAC mixtures [76]. Both degraders stabilized DCAF1 and WDR5 individually, but in opposite order: PROTAC 4 shifted WDR5 more than DCAF1 (+8.9 versus +5.3 °C), whereas PROTAC 5 showed the reverse (+11.8 versus +5.9 °C) (Figure 4(C)). Changes in the mixed-protein profiles were interpreted alongside SPR and crystallography, which supplied independent evidence of complex formation. PROTAC 5, with by far the largest DCAF1 shift of the series, formed a ternary complex by SPR yet degraded neither exogenous nor endogenous WDR5 in cells, whereas PROTAC 4, whose DCAF1 shift was less than half as large, was the most effective of the DCAF1 degraders reported in the study.

A closely related nanoDSF precedent exists for molecular glues: FR900359 and YM-254890 produced concentration-dependent stabilization and converted the biphasic unfolding profile of purified Gα11–Gβγ into a monophasic transition, consistent with stabilization of the subunit interface [86]. Together, these examples support using nanoDSF to select constructs and assay conditions with reproducible thermal profiles and limited aggregation. This selection concerns sample suitability; it does not rank affinity, cooperativity or degradation efficacy. Table 1 translates this supporting role into a hypothetical experiment, explaining how binary controls, recruitment controls and concentration series address alternative interpretations of mixed-protein profiles. SPR, ITC, NanoBRET, native mass spectrometry [87] and structural analysis provide complementary evidence, while ubiquitination and degradation require dedicated functional and cellular assays.

### 4.4. Nucleic acids and protein–RNA complexes

RNA-binding proteins (RBPs) control precursor messenger RNA processing, RNA stability, localization and translation, and also mediate recognition of viral or aberrantly modified RNA [88–90]. Their biological reach, together with growing efforts to disrupt or stabilize protein-RNA interfaces, makes them an emerging drug-discovery target class [91]. For these targets, nanoDSF can report the conformational consequences of RNA or compound association with the protein. Because the signal arises mainly from the protein, however, it does not directly measure RNA melting.

A useful proof of concept was provided by Sikorska et al., who examined full-length retinoic acid-inducible gene I (RIG-I) rather than the isolated C-terminal domain. Apo RIG-I unfolded at 46.6°C, whereas four double-stranded RNA ligands increased the apparent melting temperature to 53.7–59.6°C; within matched hairpins, 5′-triphosphorylated RNA stabilized RIG-I more than its 5′-OH counterpart (57.7 versus 53.7 °C). Adenosine diphosphate (ADP) or the non-hydrolysable adenosine triphosphate analogue adenosine 5′-(β,γ-methylene)triphosphate produced little further change, while the ADP–aluminum fluoride complex broadened the transitions and shifted their inflection points to 63.9–67.6°C. Together with NMR and MST, these profiles were interpreted as RNA-driven

Table 1. A hypothetical nanoDSF experiment to investigate the thermal consequences of PROTAC-mediated ternary assembly. The comparisons in steps 3 and 4 require matched protein concentrations and assay conditions. Expected ternary profiles should not be constructed by adding $\Delta T_m$ values or F350/F330 ratios.

| Step and comparison | Illustrative observation | Logic of the comparison | Remaining limitation |
|---|---|---|---|
| 1. Qualify the readout: buffer, PROTAC alone, POI alone and E3 alone; inspect fluorescence, absorbance and scattering | Both proteins provide interpretable profiles, without substantial compound interference or pre-transition aggregation | Establish that subsequent comparisons can be interpreted | Little compound fluorescence does not exclude inner-filter attenuation |
| 2. Define binary effects: POI ± PROTAC and E3 ± PROTAC | The POI transition shifts; the E3 profile changes little despite independently confirmed binding | Identify effects that require only one partner and recognize thermally silent binding | Neither the presence nor absence of a shift establishes affinity |
| 3. Examine the mixture: POI + E3 ± PROTAC, alongside binary controls measured in parallel | The complete sample shows a new or shifted transition, or a previously resolved transition is no longer distinguishable | Identify a response whose dependence on recruitment can be tested | Binary occupancy changes, optical interference or aggregation can alter the profile without ternary assembly (false positive). |
| 4. Test the requirement for linked engagement: unlinked warheads and a recruitment-deficient analogue, with matched binary controls | The additional feature disappears, while the POI binary effect remains | Distinguish linker-dependent assembly from the combined effect of two independent binary interactions | Control binding and optical properties must be verified; similar profiles do not exclude different molecular assemblies |
| 5. Test concentration dependence: titrate PROTAC and, where needed, vary the POI:E3 ratio | The feature is reproducible across a defined concentration range | Check that the interpretation is not restricted to one arbitrary mixture | Concentration-dependent interference can mimic a response; the shape of the dependence is not diagnostic, and a hook-shaped thermal response is neither required nor diagnostic of ternary-complex formation |
| 6. Check ternary formation independently: use a ternary-specific SPR or TR-FRET assay under comparable conditions | Assembly is detected with the intact PROTAC and reduced by the recruitment control | Test whether the thermal interpretation agrees with an independent measurement of ternary assembly. | An independently confirmed ternary complex may produce no detectable thermal change, or its thermal effects may be masked by overlapping transitions (false negative). Assembly alone does not establish productive ubiquitination or degradation. |

conformational rearrangements involving the C-terminal and helicase regions, rather than as a direct measure of RNA affinity or release of the caspase activation and recruitment domains. The study illustrates how nanoDSF can distinguish RNA-protein states through their conformational consequences [92].

The value for chemical discovery is illustrated by a 2025 study of the $N^6$-methyladenosine ($m^6A$) reader YTH domain-containing family protein 2 (YTHDF2). Qiu et al. used nanoDSF in an orthogonal cascade after fluorescence polarization, AlphaScreen and electrophoretic mobility shift assay experiments had identified phenylpyrazoles that disrupted the YTHDF2-$m^6A$-RNA interaction. Seven compounds stabilized the purified YT521-B homology domain and CK-75 produced a $\Delta T_m$ of 2.08°C at 10 µM. Direct binding was subsequently quantified by MST ($K_D = 26.2 \pm 2.3$ µM) and supported in cells by a 2.4°C CETSA shift. This is a useful model for positioning nanoDSF: not as a stand-alone assay of protein-RNA disruption, but as a rapid, label-free confirmation that an active compound also engages and stabilizes the RBP itself [93]. NanoDSF can also serve as an assay-qualification step in RBP workflows: for interferon-induced proteins with tetratricopeptide repeats 1–3, simultaneous intrinsic-fluorescence and dynamic light scattering (DLS) measurements defined unfolding and aggregation limits before MST and biolayer-interferometry studies of protein and RNA complexes [94]. For such applications, compare protein-only, RNA-only, protein–RNA, protein–compound and protein–RNA–compound samples under matched conditions, ideally with titrations. RNA-dependent thermal responses should then be assessed alongside direct measurements of protein–RNA association and target function.

## 5. Current limitations and technical bottlenecks

### 5.1. Intrinsic-fluorophore dependence

Nucleophosmin 1 (NPM1) is a multifunctional nucleolar protein involved in cell growth, ribosome biogenesis and cell-cycle regulation. In acute myeloid leukemia (AML), recurrent exon 12 frameshift mutations alter the extreme C-terminus of NPM1. The most common type A mutation, p.W288Cfs *12, exemplifies this mechanism: the frameshift replaces the native C-terminal sequence and results in the loss of both W288 and W290, whereas other AML-associated variants may retain W288 but lose W290 (Figure 5(A)) [96]. These tryptophans form part of the hydrophobic core and nucleolar localization signal of the folded C-terminal three-helix bundle (approximately residues 243–294). Their loss destabilizes the domain and, together with acquisition of a new nuclear export signal, promotes aberrant cytoplasmic localization of mutant NPM1

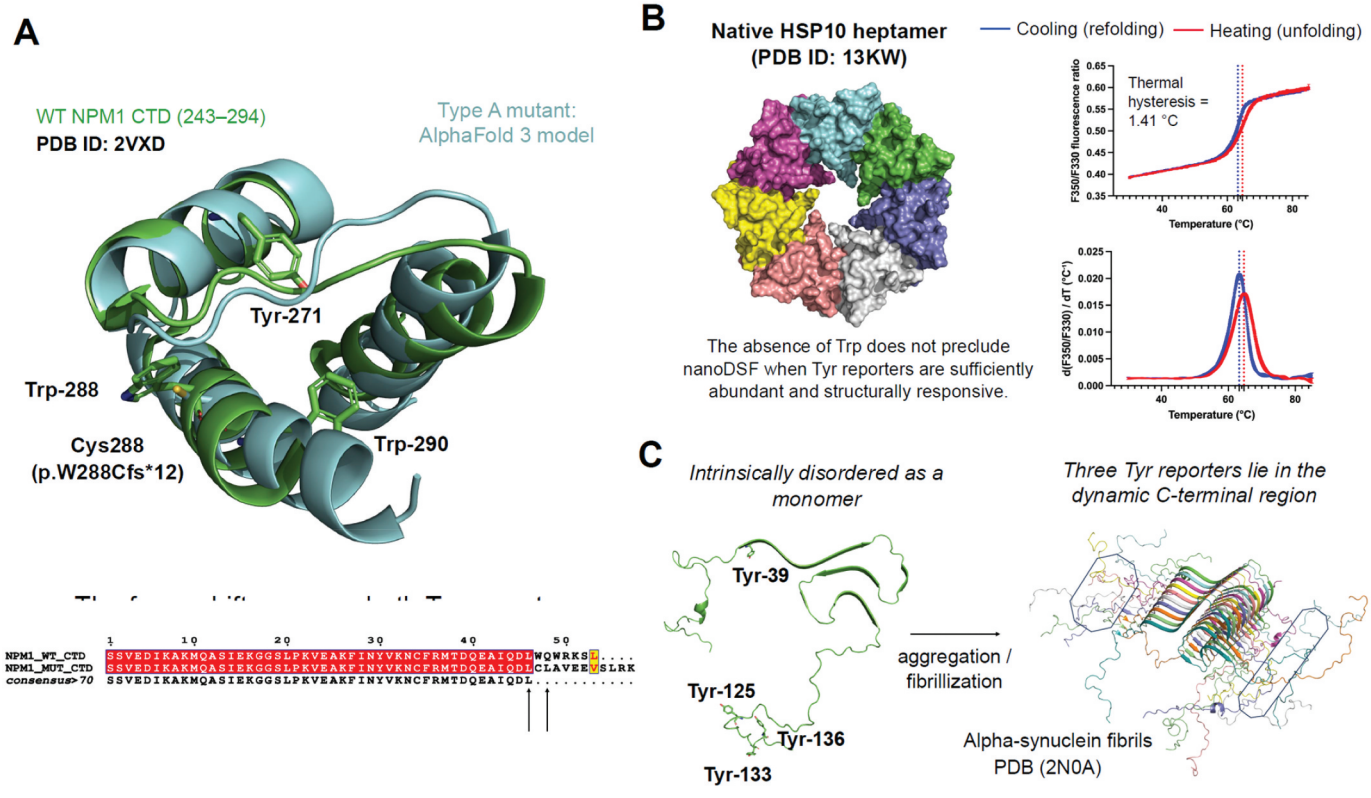



Figure 5. Intrinsic fluorophore dependence and structural context as determinants of assay suitability. (A) Solution NMR structure of wild-type NPM1 C-terminal domain (CTD; PDB: 2VXD, green ribbon representation), highlighting Tyr271, Trp288, and Trp290, compared with an illustrative AlphaFold 3 model (cyan ribbon representation) of the acute myeloid leukaemia p.W288Cfs *12 mutant. The frameshift replaces the native C-terminal sequence and abolishes both Trp reporters as indicated by the arrows, limiting its use in nanoDSF. (B) Human HSP10 forms a single heptameric ring (PDB: 13 KW) containing three Tyr residues per subunit (21 Tyr per heptamer). At 10 µM heptamer, measurable heating and cooling transitions are produced. Triplicate capillary analysis yielded inflection points of 64.65 ± 0.04°C during heating and 63.24 ± 0.02°C during cooling, corresponding to a thermal hysteresis of 1.41°C. The nanoDSF traces were replotted with permission from data provided by Larsson et al. [95]. (C) α-Synuclein contains four Tyr residues but no Trp and is intrinsically disordered as a monomer. Fibril formation generates an ordered cross-β core (PDB: 2N0A), but the Tyr reporters remain predominantly within dynamic regions outside that core; fibrillisation alone therefore does not yield a reversible, cooperative nanoDSF transition. Structures and nanoDSF data were derived from the sources indicated in [95–99].

[100]. This provides a particularly instructive example of intrinsic-fluorophore dependence in nanoDSF. Whereas the wild-type C-terminal domain contains two strategically positioned tryptophans, AML-associated mutants that lose both residues would leave Y271 as the only intrinsic Tyr/Trp fluorophore within this folded domain. Consequently, the fluorescence signal available to report its unfolding would be markedly reduced, potentially making label-free nanoDSF poorly informative for this specific construct despite its biological and therapeutic relevance. A dye-based screening precedent is also available for NPM1: a SYPRO Orange DSF screen of the wild-type C-terminal domain identified 25 stabilizing compounds from a 2,560-member library, after which the leading hits were evaluated by SPR, intrinsic fluorescence and cellular assays [101]. This study concerns the wild-type domain rather than the Trp-depleted mutants discussed above. Loss of aromatic reporters in a mutant should, however, be distinguished from the absence of tryptophan in the native sequence. An example is provided by the recent study by He et al. on the blood-brain barrier-penetrant KRAS G12C inhibitor JMKX1899, also known as sosimerasib, a selective small-molecule inhibitor currently under clinical development for KRAS G12C-mutated non-small-cell lung cancer with brain metastases. In that work, thermal stability experiments were performed on guanosine diphosphate (GDP)-loaded KRAS G12C using a Prometheus NT.48 instrument and 10 µL of unlabeled samples. JMKX1899 produced an approximately 18°C increase in the apparent $T_m$ of GDP-loaded KRAS G12C in two independent experiments, each with three replicates [102]. The native KRAS sequence lacks Trp, thus Tyr residues may contribute to the reported intrinsic-fluorescence response, although their individual contributions were not established in the study. A complementary example is human heat shock protein 10 (HSP10), whose native sequence contains no Trp and three Tyr residues per subunit. Larsson et al. observed measurable heating and cooling transitions in a recombinant HSP10 preparation (Figure 5(B)) [95]. Together, these cases show that native Trp is not an absolute requirement. Suitability depends on whether the construct produces a measurable, interpretable intrinsic-fluorescence transition.

### 5.2. Non-canonical melting and assembly profiles

For multidomain proteins, sensitivity depends on the number, location and environmental response of tryptophan and tyrosine residues. A transition in a domain without an informative aromatic reporter may be attenuated, merged or missed. Dye-based DSF is also weighted by hydrophobic exposure and dye accessibility. Neither method resolves every domain transition; interpretation should consider sequence, domain architecture and structure.

In intrinsically disordered proteins, an aromatic signal does not necessarily provide a cooperative unfolding readout. α-Synuclein, for example, contains four tyrosine residues but no tryptophan; some studies have introduced a Y39W mutation to monitor aggregation through intrinsic fluorescence [103]. A reporter for aggregation does not, however, establish that the protein undergoes a reversible, cooperative thermal unfolding transition (Figure 5(C)) [104]. Tau provides another elegant example: the longest neuronal isoform, Tau-40, contains five tyrosine residues but no tryptophan. Despite its biological relevance to pathological aggregation in Alzheimer's disease, tau is poorly suited to a conventional nanoDSF analysis based on a well-defined fluorescence transition and melting temperature. Nevertheless, intrinsic Tyr fluorescence has been used to follow ligand-induced spectral changes in full-length tau and in its four-repeat domain, which contains a single native Tyr; these responses should not be interpreted as cooperative thermal unfolding [105,106]. Thus, for intrinsically disordered proteins, suitability for nanoDSF depends not only on tryptophan and tyrosine content, but also on whether heating produces a reproducible fluorescence change that can be assigned to a biologically meaningful structural transition. Not all non-canonical thermal profiles, however, represent an assay limitation. Unlike intrinsically disordered tau and α-synuclein, tubulin is a folded α/β heterodimer that undergoes regulated temperature-dependent polymerization. Baksheeva et al. exploited nanoDSF to monitor both compound binding and shifts in tubulin polymerization temperature. Screening 1,520 approved compounds recovered established microtubule-targeting agents and identified additional polymerization modulators, illustrating how nanoDSF can couple target engagement with a functional assembly readout [47].

### 5.3. Irreversible aggregation

Thermal unfolding may also lead to irreversible aggregation. In that case the transition observed will reflect the kinetics of unfolding and aggregation rather than equilibrium stability. Aggregates have two effects: they affect the fluorescence signal by scattering and attenuation, and they change the emission itself, since in irreversibly unfolding α-amylases aggregation significantly reduces the tryptophan red shift that accompanies unfolding [107]. If aggregation starts before or during the fluorescence transition, the apparent $T_m$ may reflect several overlapping processes, and the value extracted under these conditions should not be seen as an equilibrium measure of stabilization.

Where aggregation follows a clear and reproducible fluorescence transition, an apparent $T_m$ may still support comparisons under matched experimental conditions. The separation of fluorescence and scattering transitions does not, however, demonstrate that unfolding is reversible. We therefore recommend checking the raw F330, F350, their ratio and the scattering trace together, and reexamining ambiguous profiles at lower protein concentration and slower heating rates: in irreversible systems both the transition temperature and the magnitude of the red shift depend on these parameters, and conditions that reduce aggregation restore the expected spectral behavior [107]. Where aggregation obscures the transition altogether, the result is better reported as uninterpretable under the conditions tested and pursued with an independent method. The NISTmAb study discussed in Section 4.2 reinforces this distinction: its combined nanoDSF, differential scanning calorimetry and hydrogen–deuterium exchange mass spectrometry analysis shows why conformational stability and aggregation propensity should be assessed separately [71].

Table 2. Software and open resources for the acquisition, fitting, and quality control of nanoDSF and related thermal-shift data.

| Resource and access | nanoDSF compatibility | Recommended use and main caution | Reference |
|---|---|---|---|
| PR.ThermControl / PR.Panta Control *Proprietary* | Direct: instrument acquisition | Set up thermal scans and inspect F330, F350, the fluorescence ratio, and turbidity or scattering. Automatically assigned transitions must be checked against the raw traces. | NanoTemper documentation |
| PR.Stability Analysis / PR. Panta Analysis *Proprietary* | Direct: vendor analysis | Merge runs and replicates, compare conditions, define regions of interest and export results. Report the software version, exclusions and any manual changes. | NanoTemper documentation |
| MoltenProt / eSPC *Open source; web or local* | Direct: Prometheus exports supported | Fit equilibrium thermodynamic, kinetic and empirical unfolding models and obtain $T_m$, $T_{onset}$, ΔH and apparent ΔG. Inspect fit quality and match model choice to reversible versus irreversible unfolding behavior. | [31,110] |
| FoldAffinity *Open source; web or local* | Direct: nanoDSF titrations | Estimate $K_D$ by isothermal analysis of ligand titrations. A suitable concentration series and unfolding model are required, and the estimate should be confirmed by an orthogonal method. | [111] |
| TPPU_DSF *Free, open-source web tool* | Indirect: developed for plate DSF (qPCR-format exports) | Calculate $T_m$ and apparent thermodynamic parameters of unfolding, including Gibbs free energy (ΔG°u), enthalpy (ΔH°u), and entropy (ΔS°u), from temperature-versus-signal data. Check fit quality and the assumptions concerning reversibility before interpreting thermodynamic parameters. A validated Prometheus import workflow has not been reported. | [112] |
| DSFworld / DSFbase *Open-source web tool and dataset* | Indirect: developed for plate DSF | Fit unusual curves, including multiple transitions and signal decay. DSFworld was benchmarked against DSFbase, an open dataset of experimental curves. Direct Prometheus import has not been validated. | [109] |
| ShiftScan *Open source stand-alone tool* | Indirect: developed for high-throughput plate DSF | Automate curve triage, $T_m$ assignment and hit prioritization. It provides a useful model for future nanoDSF quality control but is not a validated Prometheus workflow. | [50] |
| ProThermDB *Open database* | Contextual resource | Retrieve $T_m$, ΔG, ΔH, ΔCp, mutations, methods and solution conditions. Quantitative comparisons require matched constructs and conditions because the records are heterogeneous. | [113] |

Abbreviations: 1,8-ANS, 1-anilinonaphthalene-8-sulfonic acid; ADP, adenosine diphosphate; AML, acute myeloid leukemia; APF, L-Ala–L-Pro–L-Phe; CETSA, cellular thermal shift assay; CH2, second constant domain of the immunoglobulin heavy chain; CH3, third constant domain of the immunoglobulin heavy chain; CTD, C-terminal domain; $C_{1/2}$, midpoint of chemical denaturation; DCAF1, DDB1- and CUL4-associated factor 1; DDM, n-dodecyl-β-D-maltoside; DLS, dynamic light scattering; DMSO, dimethyl sulfoxide; DSF, differential scanning fluorimetry; DSi-Poised, Diamond-SGC-iNEXT Poised; DYRK1A, dual-specificity tyrosine-phosphorylation-regulated kinase 1A; E3, E3 ubiquitin ligase; F330, fluorescence emission at 330 nm; F350, fluorescence emission at 350 nm; FBDD, fragment-based drug discovery; Fc, fragment crystallizable; FcRTAC, FcγRIIb-targeting chimera; FcγRIIb, Fc gamma receptor IIb; GDP, guanosine diphosphate; GPCR, G protein-coupled receptor; HSP10, heat shock protein 10; HTS, high-throughput screening; IgE, immunoglobulin E; IgG, immunoglobulin G; ITC, isothermal titration calorimetry; $K_D$, dissociation constant; LC–MS, liquid chromatography–mass spectrometry; LDH, lactate dehydrogenase; LMNG, lauryl maltose neopentyl glycol; $m^6A$, $N^6$-methyladenosine; MCR, multicomponent reaction; MS, mass spectrometry; MST, microscale thermophoresis; NanoBRET, NanoLuc-based bioluminescence resonance energy transfer; nanoDSF, nano differential scanning fluorimetry; NISTmAb, National Institute of Standards and Technology monoclonal antibody; NMR, nuclear magnetic resonance; NPM1, nucleophosmin 1; NS2B–NS3, nonstructural protein 2B–nonstructural protein 3; PAINS, pan-assay interference compound; PCR, polymerase chain reaction; PDB, Protein Data Bank; POI, protein of interest; PROTAC, proteolysis-targeting chimera; QC, quality control; RBD, receptor-binding domain; RBP, RNA-binding protein; RIG-I, retinoic acid-inducible gene I; RNA, ribonucleic acid; RV-A2, human rhinovirus A2; SAR, structure–activity relationship; SARS-CoV-2, severe acute respiratory syndrome coronavirus 2; SEC, size-exclusion chromatography; smFRET, single-molecule Förster resonance energy transfer; SPR, surface plasmon resonance; $T_m$, apparent melting temperature; $T_{onset}$, unfolding onset temperature; TR-FRET, time-resolved Förster resonance energy transfer; Trp, tryptophan; Tyr, tyrosine; Ub, ubiquitination; UV, ultraviolet; VDAC1, voltage-dependent anion channel 1; VHL, von Hippel–Lindau; WDR5, WD repeat-containing protein 5; WT, wild type; YTHDF2, YTH domain-containing family protein 2; ΔCp, heat-capacity change; ΔG, Gibbs free-energy change; ΔH, enthalpy change; ΔS, entropy change; $\Delta T_m$, ligand-induced change in apparent melting temperature.

### 5.4. Data-processing bottlenecks

Most commercial packages identify the apparent melting temperature from the maximum of the first derivative of the fluorescence ratio. This approach is often adequate for a single cooperative transition, but it can become misleading when a curve has high initial fluorescence, multiple transitions, as in multidomain proteins, or temperature-dependent signal decay. Fitting such profiles with a single sigmoid can therefore produce an apparent melting temperature with little mechanistic meaning. Augustijn et al. addressed this problem specifically for intrinsic-fluorescence DSF by applying simultaneous constrained non-linear fits to the fluorescence intensity, ratio and their derivatives. The method separated strongly overlapping transitions and estimated both apparent melting temperatures and unfolding onset, making it particularly relevant to nanoDSF analysis of multidomain proteins and biotherapeutics, although model choice and fit residuals still require scrutiny [108].

DSFworld subsequently introduced models for multiple transitions, high initial signal and temperature-dependent decay, benchmarked against a large collection of experimental plate-DSF curves [109], while ShiftScan automates curve triage and control-based quality assessment at plate scale [50]. A satisfactory fit does not by itself validate the underlying physical model. As discussed in Section 3 and 5.3, equilibrium thermodynamic analysis requires reversible unfolding and adequate equilibration [31]. Even apparently simple profiles may be compatible with either two-state or three-state behavior, limiting the mechanistic conclusions that can be drawn from curve shape alone. Available software and open resources for the acquisition, fitting and quality control of nanoDSF and related thermal-shift data are summarized in Table 2.

## 6. Conclusion

NanoDSF has evolved from a dye-free alternative to conventional DSF into a low-volume method for comparative analysis of protein stability, ligand-induced conformational change and aggregation. Its central advantage is not simply removal of an

extrinsic dye, but the simultaneous acquisition of intrinsic fluorescence and scattering under conditions in which dye-based measurements can fail. Dye-free, however, does not mean interference-free: the method still requires an informative aromatic signal and a measurable conformational transition, and remains vulnerable to compound absorption, fluorescence, quenching and light scattering. The evidence reviewed here supports a defined position in drug discovery. We recommend nanoDSF as a primary biophysical screen for focused and fragment libraries with reproducible thermal profiles and verified compound optical compatibility, and as a direct method for comparing constructs, formulations and membrane-protein preparations. For large screening campaigns and PROTAC programs, we recommend its complementary use alongside dedicated binding and functional assays. A thermal shift does not establish affinity, mechanism or functional engagement, and its absence does not exclude binding. Wider adoption will depend on profile-level analysis, transparent quality-control criteria, interoperable data and prospective benchmarking against downstream outcomes. Within these boundaries, nanoDSF can mature from a convenient confirmation method into a reproducible component of discovery and developability workflows.

## 7. Expert opinion

### 7.1. From a benchtop instrument to an integrated discovery module

Within the next five years, we expect nanoDSF to become part of robotic workcells combining acoustic compound dispensing, automated sample handling and thermal profiling. Plate-based intrinsic DSF, demonstrated with 10 µL samples in 384-well plates and benchmarked against calorimetry and circular dichroism, provides a technical basis for this development [114]. We do not expect capillaries to disappear; we expect them to lose their monopoly. Microplates should dominate automated screening and formulation campaigns, whereas capillaries will remain useful when maximal signal quality or flexible assay development matters more than parallelization. Automated acquisition will also require rules for routing ambiguous profiles to repeat measurements, concentration series or orthogonal assays before they influence hit selection.

### 7.2. From a single $T_m$ to decision-ready thermal fingerprints

We expect the analytical focus to shift from a single apparent $T_m$ to the full thermal profile: raw F330 and F350 traces or emission spectra, their ratio or barycentric metric, initial intensity, unfolding onset, scattering and aggregation onset, replicate agreement and concentration dependence. Tools such as ShiftScan already automate curve fitting and control-based quality checks in dye-based DSF [50]. Machine learning has also been applied to nanoDSF plasma-profile classification [115] but its use for screening quality control requires separate validation. We propose training supervised models on raw F330 and F350 traces, scattering where available, matched controls and assay metadata from multiple targets, instruments and laboratories. Expert annotations should flag interpretable transitions, multiphasic profiles, aggregation-associated changes, optical interference and unassessable measurements, and annotations of interference or aggregation should be supported by compound-only controls, absorbance or scattering measurements, or repeat experiments. Ambiguous and failed measurements should be retained rather than removed to simplify training. Model outputs should identify profiles requiring review or repeat measurement, with confidence calibrated against errors on separate validation data: a smooth fluorescence ratio accompanied by pre-transition scattering, for example, should be flagged for review rather than converted into a binding call. Failure modes include misclassifying valid multidomain profiles as artifacts, accepting interference as a clean transition, and poor performance on unfamiliar targets or instruments. Validation should use targets and laboratories excluded from training, keep all technical replicates of a sample in the same data partition, and compare performance against rule-based quality control and expert review, since simple checks can be automated without machine learning. Low-confidence predictions should trigger expert review; uninterpretable profiles should be recorded as unassessable rather than as non-binders.

### 7.3. Increasing biological complexity without losing specificity

We predict that nanoDSF will expand into more complex but experimentally defined systems, rather than become a general whole-cell target-engagement assay. Likely growth areas include multidomain biologics, membrane proteins in controlled lipid environments, protein–RNA and oligomeric assemblies and induced-proximity systems. PROTACs represent a particularly open opportunity. Dye-based DSF has shown that ternary mixtures can generate altered thermal profiles [76], whereas published nanoDSF data in degrader programs have primarily addressed construct qualification or binary ligand effects [116] rather than systematic apo–binary–ternary comparisons. We encourage its prospective use where extrinsic dyes are compromised by lipophilic degraders, detergents or lipid mimetics, provided that both protein partners produce sufficiently strong and distinguishable intrinsic transitions. Such experiments could identify preparations with reproducible thermal profiles and limited aggregation for direct ternary-complex assays. Decisions about linker performance, cooperativity and degradation would still require independent binding, ubiquitination and cellular measurements. More broadly, proteome-wide intrinsic fluorescence in intact cells lacks molecular assignment. We therefore recommend nanoDSF for defined *in vitro* screening and sample characterization, with target-specific cellular methods used to establish engagement.

### 7.4. Adoption will be determined by benchmarking, not capacity

By the early 2030s, nominal capacity will no longer be a persuasive endpoint. Progress should be judged by time

to an orthogonally validated hit, protein consumed per decision, false-positive and false-negative rates, cross-laboratory reproducibility and downstream attrition. This will require shared reference panels, interoperable raw-data exports and a minimum record covering construct identity, concentration, matrix, solvent, heating program, format, replicate structure and all exclusions or manual adjustments. Reference panels should include weak signals, multiphasic proteins, aggregation-prone samples and fluorescent or scattering compounds, rather than only ideal two-state proteins. Prospective comparisons should establish whether adding nanoDSF reduces sample consumption and unnecessary follow-up while preserving the recovery of independently validated hits and useful constructs. If automation is coupled to standardization and prospective benchmarking, nanoDSF can progress from confirming decisions to shaping them.

## Funding

The authors are funded by the European Commission under the HORIZON EUROPE Framework Programme - HORIZON EUROPE Marie Sklodowska-Curie Actions grant [no. CZ.02.01.01/00/22_010/0008685]. The authors are also funded by European Research Agency (ERA) Chair ACCELERATOR award [101087318] and the European Research Council (ERC) AMADEUS award [no. 101098001]. The authors also declare support from the Dutch Cancer Society/KWF [award no. 14712] and the Schmidt Futures ORD initiative.

## Declaration of interest

The authors have no other relevant affiliations or financial involvement with any organization or entity with a financial interest in or financial conflict with the subject matter or materials discussed in the manuscript apart from those disclosed.

In compliance with the International Committee of Medical Journal Editors (ICMJE) recommendations, the authors acknowledge the utilization of AI services in this work: the authors of this article used ChatGPT (GPT-6.1 Sol) by OpenAI exclusively for minor English corrections to improve the readability and flow of the text in this work. It was also utilized for the purposes of identifying relevant literature and to assist in the development of schematic elements of Figure 1, based on the authors' concepts and specifications. All sentences revised by GPT-6.1 Sol were reviewed and verified by the authors. No content was generated de novo or were data altered by GPT-6.1 Sol or any other AI service.

## Author contributions

CRediT: **Atilio Reyes Romero:** Investigation, Writing – original draft, Writing – review & editing; **Alexander S. S. Dömling:** Resources, Supervision, Writing – review & editing; **Matthew R. Groves:** Conceptualization, Supervision, Writing – original draft, Writing – review & editing.

## Reviewer disclosures

Peer reviewers on this manuscript have no relevant financial or other relationships to disclose.

## References

**Papers of special note have been highlighted as either of interest (•) or of considerable interest (••) to readers.**

1. Higueruelo AP, Jubb H, Blundell TL. Protein-protein interactions as druggable targets: recent technological advances. Curr Opin Pharmacol. 2013;13(5):791–796. doi: 10.1016/j.coph.2013.05.009
2. Arkin MR, Wells JA. Small-molecule inhibitors of protein-protein interactions: progressing towards the dream. Nat Rev Drug Discov. 2004;3(4):301–317. doi: 10.1038/nrd1343
3. Berg T. Modulation of protein-protein interactions with small organic molecules. Angew Chem Int Ed Engl. 2003;42 (22):2462–2481. doi: 10.1002/anie.200200558
4. Camps-Fajol C, Cavero D, Minguillón J, et al. Targeting protein-protein interactions in drug discovery: modulators approved or in clinical trials for cancer treatment. Pharmacol Res. 2025;211:107544. doi: 10.1016/j.phrs.2024.107544
5. Whitfield JR, Soucek L. Myc in cancer: from undruggable target to clinical trials. Nat Rev Drug Discov. 2025;24(6):445–457. doi: 10.1038/s41573-025-01143-2
6. Prior IA, Hood FE, Hartley JL. The frequency of Ras mutations in cancer. Cancer Res. 2020;80(14):2969–2974. doi: 10.1158/0008-5472.CAN-19-3682
7. Morstein J, Bowcut V, Fernando M, et al. Targeting ras-, rho-, and rab-family GTPases via a conserved cryptic pocket. Cell. 2024;187 (22):6379–6392.e17. doi: 10.1016/j.cell.2024.08.017
8. Renaud J-P, Chung C-W, Danielson UH, et al. Biophysics in drug discovery: impact, challenges and opportunities. Nat Rev Drug Discov. 2016;15(10):679–698. doi: 10.1038/nrd.2016.123
9. Pantoliano MW, Petrella EC, Kwasnoski JD, et al. High-density miniaturized thermal shift assays as a general strategy for drug discovery. J Biomol Screen. 2001;6(6):429–440. doi: 10.1177/108705710100600609
10. Lo M-C, Aulabaugh A, Jin G, et al. Evaluation of fluorescence-based thermal shift assays for hit identification in drug discovery. Anal Biochem. 2004;332(1):153–159. doi: 10.1016/j.ab.2004.04.031
11. Niesen FH, Berglund H, Vedadi M. The use of differential scanning fluorimetry to detect ligand interactions that promote protein stability. Nat Protoc. 2007;2(9):2212–2221. doi: 10.1038/nprot.2007.321
• **Sets out a foundational dye-based DSF protocol for detecting ligand-induced changes in protein thermal stability.**
12. Ericsson UB, Hallberg BM, DeTitta GT, et al. Thermofluor-based high-throughput stability optimization of proteins for structural studies. Anal Biochem. 2006;357(2):289–298. doi: 10.1016/j.ab.2006.07.027
13. Vedadi M, Niesen FH, Allali-Hassani A, et al. Chemical screening methods to identify ligands that promote protein stability, protein crystallization, and structure determination. Proc Natl Acad Sci U S A. 2006;103(43):15835–15840. doi: 10.1073/pnas.0605224103
14. Boivin S, Kozak S, Meijers R. Optimization of protein purification and characterization using Thermofluor screens. Protein Expr Purif. 2013;91(2):192–206. doi: 10.1016/j.pep.2013.08.002
15. Prabhu N, Dai L, Nordlund P. CETSA in integrated proteomics studies of cellular processes. Curr Opin Chem Biol. 2020;54:54–62. doi: 10.1016/j.cbpa.2019.11.004
16. Martinez Molina D, Jafari R, Ignatushchenko M, et al. Monitoring drug target engagement in cells and tissues using the cellular thermal shift assay. Science. 2013;341(6141):84–87. doi: 10.1126/science.1233606
17. Simeonov A. Recent developments in the use of differential scanning fluorometry in protein and small molecule discovery and characterization. Expert Opin Drug Discov. 2013;8(9):1071–1082. doi: 10.1517/17460441.2013.806479
18. Real-Hohn A, Groznica M, Löffler N, et al. nanoDSF: in vitro label-free method to monitor picornavirus uncoating and test compounds affecting particle stability. Front Microbiol. 2020;11:1442. doi: 10.3389/fmicb.2020.01442

19. Kotov V, Killer M, Jungnickel KEJ, et al. Plasticity of the binding pocket in peptide transporters underpins promiscuous substrate recognition. Cell Rep. 2023;42(8):112831. doi: 10.1016/j.celrep.2023.112831
20. Gao K, Oerlemans R, Groves MR. Theory and applications of differential scanning fluorimetry in early-stage drug discovery. Biophys Rev. 2020;12(1):85–104. doi: 10.1007/s12551-020-00619-2
21. Hawe A, Sutter M, Jiskoot W. Extrinsic fluorescent dyes as tools for protein characterization. Pharm Res. 2008;25(7):1487–1499. doi: 10.1007/s11095-007-9516-9
22. Baell JB, Holloway GA. New substructure filters for removal of pan assay interference compounds (pains) from screening libraries and for their exclusion in bioassays. J Med Chem. 2010;53(7):2719–2740. doi: 10.1021/jm901137j
23. Kranz JK, Schalk-Hihi C. Protein thermal shifts to identify low molecular weight fragments. Methods Enzymol. 2011;493:277–298. doi: 10.1016/B978-0-12-381274-2.00011-X
24. Kroeger T, Frieg B, Zhang T, et al. EDTA aggregates induce SYPRO orange-based fluorescence in thermal shift assay. PLOS ONE. 2017;12(5):e0177024. doi: 10.1371/journal.pone.0177024
25. Alexandrov AI, Mileni M, Chien EYT, et al. Microscale fluorescent thermal stability assay for membrane proteins. Structure. 2008;16(3):351–359. doi: 10.1016/j.str.2008.02.004
26. Wu T, Yu JC, Suresh A, et al. Protein-adaptive differential scanning fluorimetry using conformationally responsive dyes. Nat Biotechnol. 2025;43(1):106–113. doi: 10.1038/s41587-024-02158-7
27. Fonin AV, Sulatskaya AI, Kuznetsova IM, et al. Fluorescence of dyes in solutions with high absorbance. Inner filter effect correction. PLOS ONE. 2014;9(7):e103878. doi: 10.1371/journal.pone.0103878
28. Ahmad MUD, Fish A, Molenaar J, et al. Nano-differential scanning fluorimetry for screening in fragment-based lead discovery. J Vis Exp. 2021;171:e62469. doi: 10.3791/62469
•• **Details a robotics-assisted nanoDSF workflow for fragment screening and pairs intrinsic-fluorescence measurements with back-scattering to assess sample quality.**
29. Magnusson AO, Szekrenyi A, Joosten H-J, et al. nanoDSF as screening tool for enzyme libraries and biotechnology development. FEBS J. 2019;286(1):184–204. doi: 10.1111/febs.14696
30. Hansel CS, Lanne A, Rowlands H, et al. High-throughput differential scanning fluorimetry (DSF) and cellular thermal shift assays (CETSA): shifting from manual to automated screening. SLAS Technol. 2023;28(6):411–415. doi: 10.1016/j.slast.2023.08.004
31. Kotov V, Mlynek G, Vesper O, et al. In-depth interrogation of protein thermal unfolding data with MoltenProt. Protein Sci. 2021;30(1):201–217. doi: 10.1002/pro.3986
• **Introduces MoltenProt for fitting thermal-unfolding profiles with explicit models and extracting information beyond a single melting temperature.**
32. Kotov V, Bartels K, Veith K, et al. High-throughput stability screening for detergent-solubilized membrane proteins. Sci Rep. 2019;9(1):10379. doi: 10.1038/s41598-019-46686-8
•• **Establishes a systematic detergent screen for solubilised membrane proteins using intrinsic-fluorescence transitions and aggregation readouts.**
33. Bruch EM, Zhu S, Szymkowicz L, et al. Structural and biochemical rationale for beta variant protein booster vaccine broad cross-neutralization of SARS-CoV-2. Sci Rep. 2024;14(1):2038. doi: 10.1038/s41598-024-52499-1
34. Waldron TT, Murphy KP. Stabilization of proteins by ligand binding: application to drug screening and determination of unfolding energetics. Biochemistry. 2003;42(17):5058–5064. doi: 10.1021/bi034212v
35. Cimmperman P, Baranauskiene L, Jachimoviciūte S, et al. A quantitative model of thermal stabilization and destabilization of proteins by ligands. Biophys J. 2008;95(7):3222–3231. doi: 10.1529/biophysj.108.134973
•• **Develops a thermodynamic model that incorporates ligand binding to native and denatured states and accounts for both positive and negative thermal shifts.**
36. Matulis D, Kranz JK, Salemme FR, et al. Thermodynamic stability of carbonic anhydrase: measurements of binding affinity and stoichiometry using ThermoFluor. Biochemistry. 2005;44(13):5258–5266. doi: 10.1021/bi048135v
37. Erlanson DA, Fesik SW, Hubbard RE, et al. Twenty years on: the impact of fragments on drug discovery. Nat Rev Drug Discov. 2016;15(9):605–619. doi: 10.1038/nrd.2016.109
38. Murray CW, Rees DC. The rise of fragment-based drug discovery. Nat Chem. 2009;1(3):187–192. doi: 10.1038/nchem.217
39. Grosjean H, Biggin PC. Developments and challenges in hit progression within fragment-based drug discovery. Nat Commun. 2026;17(1):2226. doi: 10.1038/s41467-026-68941-z
40. Kaltheuner IH, Anand K, Moecking J, et al. Abemaciclib is a potent inhibitor of DYRK1A and hip kinases involved in transcriptional regulation. Nat Commun. 2021;12(1):6607. doi: 10.1038/s41467-021-26935-z
41. Thabault L, Brustenga C, Savoyen P, et al. Discovery of small molecules interacting at lactate dehydrogenases tetrameric interface using a biophysical screening cascade. Eur J Med Chem. 2022;230:114102. doi: 10.1016/j.ejmech.2022.114102
•• **Places intrinsic-fluorescence thermal profiling at the start of a biophysical screening cascade for compounds targeting lactate dehydrogenase oligomerisation interfaces.**
42. Gao K, Shaabani S, Xu R, et al. Nanoscale, automated, high throughput synthesis and screening for the accelerated discovery of protein modifiers. RSC Med Chem. 2021;12(5):809–818. doi: 10.1039/D1MD00087J
43. Dötsch L, Davies C, Hennes E, et al. Discovery of the sEH inhibitor epoxykynin as a potent kynurenine pathway modulator. J Med Chem. 2024;67(6):4691–4706. doi: 10.1021/acs.jmedchem.3c02245
44. Gorny H, Mularoni A, Delcros J-G, et al. Combining nano-differential scanning fluorimetry and microscale thermophoresis to investigate VDAC1 interaction with small molecules. J Enzym Inhib Med Chem. 2023;38(1):2121821. doi: 10.1080/14756366.2022.2121821
• **Combines nanoDSF and microscale thermophoresis to examine small-molecule interactions with the membrane protein VDAC1.**
45. Kozielski F, Sele C, Talibov VO, et al. Identification of fragments binding to SARS-CoV-2 nsp10 reveals ligand-binding sites in conserved interfaces between nsp10 and nsp14/nsp16. RSC Chem Biol. 2022;3(1):44–55. doi: 10.1039/d1cb00135c
46. Santhana Kumar K, Brunner C, Schuster M, et al. Discovery of a small molecule ligand of FRS2 that inhibits invasion and tumor growth. Cell Oncol (Dordr). 2023;46(2):331–356. doi: 10.1007/s13402-022-00753-x
47. Baksheeva V, La Rocca R, Allegro D, et al. NanoDSF screening for anti-tubulin agents uncovers new structure-activity insights. J Med Chem. 2025;68(16):17485–17498. doi: 10.1021/acs.jmedchem.5c01008
48. Gardell SJ, Hopf M, Khan A, et al. Boosting NAD+ with a small molecule that activates NAMPT. Nat Commun. 2019;10(1):3241. doi: 10.1038/s41467-019-11078-z
49. Ronzetti MH, Baljinnyam B, Itkin Z, et al. Application of temperature-responsive HIS-tag fluorophores to differential scanning fluorimetry screening of small molecule libraries. Front Pharmacol. 2022;13:1040039. doi: 10.3389/fphar.2022.1040039
50. Waterworth SC, Shenoy SR, Sharma ND, et al. ShiftScan: a tool for rapid analysis of high-throughput differential scanning fluorimetry data and compound prioritization. Protein Sci. 2025;34(3):1–13. doi: 10.1002/pro.70055
• **Introduces automated curve analysis and control-based quality checks for high-throughput dye-based DSF datasets.**
51. Capuzzi SJ, Muratov EN, Tropsha A. Phantom pains: problems with the utility of alerts for pan-assay interference compounds. J Chem Inf Model. 2017;57(3):417–427. doi: 10.1021/acs.jcim.6b00465
52. Irwin JJ, Duan D, Torosyan H, et al. An aggregation advisor for ligand discovery. J Med Chem. 2015;58(17):7076–7087. doi: 10.1021/acs.jmedchem.5b01105

53. Valenti D, Neves JF, Cantrelle F-X, et al. Set-up and screening of a fragment library targeting the 14-3-3 protein interface. Medchemcomm. 2019;10(10):1796–1802. doi: 10.1039/C9MD00215D
54. Wu T, Hornsby M, Zhu L, et al. Protocol for performing and optimizing differential scanning fluorimetry experiments. Star Protoc. 2023;4(4):102688. doi: 10.1016/j.xpro.2023.102688
55. Simeonov A, Jadhav A, Thomas CJ, et al. Fluorescence spectroscopic profiling of compound libraries. J Med Chem. 2008;51(8):2363–2371. doi: 10.1021/jm701301m
56. Proj M, Hrast M, Knez D, et al. Fragment-sized thiazoles in fragment-based drug discovery campaigns: friend or foe? ACS Med Chem Lett. 2022;13(12):1905–1910. doi: 10.1021/acsmedchemlett.2c00429
57. Dahlin JL, Nissink JWM, Strasser JM, et al. Pains in the assay: chemical mechanisms of assay interference and promiscuous enzymatic inhibition observed during a sulfhydryl-scavenging HTS. J Med Chem. 2015;58(5):2091–2113. doi: 10.1021/jm5019093
58. Schön A, Clarkson BR, Jaime M, et al. Temperature stability of proteins: analysis of irreversible denaturation using isothermal calorimetry. Proteins. 2017;85(11):2009–2016. doi: 10.1002/prot.25354
59. Schön A, Brown RK, Hutchins BM, et al. Ligand binding analysis and screening by chemical denaturation shift. Anal Biochem. 2013;443(1):52–57. doi: 10.1016/j.ab.2013.08.015
60. Ross P, Weihofen W, Siu F, et al. Isothermal chemical denaturation to determine binding affinity of small molecules to G-protein coupled receptors. Anal Biochem. 2015;473:41–45. doi: 10.1016/j.ab.2014.11.019
61. Bhayani JA, Ballicora MA. Determination of dissociation constants of protein ligands by thermal shift assay. Biochem Biophys Res Commun. 2022;590:1–6. doi: 10.1016/j.bbrc.2021.12.041
62. Chattopadhyay G, Varadarajan R. Facile measurement of protein stability and folding kinetics using a nano differential scanning fluorimeter. Protein Sci. 2019;28(6):1127–1134. doi: 10.1002/pro.3622
63. Hall J. A simple model for determining affinity from irreversible thermal shifts. Protein Sci. 2019;28(10):1880–1887. doi: 10.1002/pro.3701
64. Maus H, Hammerschmidt SJ, Hinze G, et al. The effects of allosteric and competitive inhibitors on ZIKV protease conformational dynamics explored through smFRET, nanoDSF, DSF, and 19F NMR. Eur J Med Chem. 2023;258:115573. doi: 10.1016/j.ejmech.2023.115573
65. Flayhan A, Mertens HDT, Ural-Blimke Y, et al. Saposin lipid nanoparticles: a highly versatile and modular tool for membrane protein research. Structure. 2018;26(2):345–355.e5. doi: 10.1016/j.str.2018.01.007
66. Selvasingh JA, McDonald EF, Neufer PD, et al. Dark nanodiscs for evaluating membrane protein thermostability by differential scanning fluorimetry. Biophys J. 2024;123(1):68–79. doi: 10.1016/j.bpj.2023.11.019
67. Beckner RL, Zoubak L, Hines KG, et al. Probing thermostability of detergent-solubilized CB2 receptor by parallel G protein-activation and ligand-binding assays. J Biol Chem. 2020;295(1):181–190. doi: 10.1074/jbc.RA119.010696
68. Wen J, Lord H, Knutson N, et al. Nano differential scanning fluorimetry for comparability studies of therapeutic proteins. Anal Biochem. 2020;593:113581. doi: 10.1016/j.ab.2020.113581
69. Kim SH, Yoo HJ, Park EJ, et al. Nano differential scanning fluorimetry-based thermal stability screening and optimal buffer selection for immunoglobulin G. Pharmaceuticals (Basel). 2021;15(1):29. doi: 10.3390/ph15010029
70. Bailly M, Mieczkowski C, Juan V, et al. Predicting antibody developability profiles through early stage discovery screening. MAbs. 2020;12(1):1743053. doi: 10.1080/19420862.2020.1743053
71. Hamuro Y, Derebe MG, Venkataramani S, et al. The effects of intramolecular and intermolecular electrostatic repulsions on the stability and aggregation of NISTmAb revealed by HDX-MS, DSC, and nanoDSF. Protein Sci. 2021;30(8):1686–1700. doi: 10.1002/pro.4129

**•• Integrates nanoDSF, differential scanning calorimetry and hydrogen–deuterium exchange mass spectrometry to distinguish conformational stability from aggregation behaviour in NISTmAb.**

72. Joshi S, Maharana C, Rathore AS. An application of nano differential scanning fluorimetry for higher order structure assessment between mAb originator and biosimilars: trastuzumab and rituximab as case studies. J Pharm Biomed Anal. 2020;186:113270. doi: 10.1016/j.jpba.2020.113270
73. Beckley NS, Lazzareschi KP, Chih H-W, et al. Investigation into temperature-induced aggregation of an antibody drug conjugate. Bioconjug Chem. 2013;24(10):1674–1683. doi: 10.1021/bc400182x
74. Kaempffe A, Dickgiesser S, Rasche N, et al. Effect of conjugation site and technique on the stability and pharmacokinetics of antibody-drug conjugates. J Pharm Sci. 2021;110(12):3776–3785. doi: 10.1016/j.xphs.2021.08.002
75. Lisina S, Inam W, Huhtala M, et al. Nano differential scanning fluorimetry as a rapid stability assessment tool in the nanoformulation of proteins. Pharmaceutics. 2023;15(5):1473. doi: 10.3390/pharmaceutics15051473
76. Mabanglo MF, Wilson B, Noureldin M, et al. Crystal structures of DCAF1-PROTAC-WDR5 ternary complexes provide insight into DCAF1 substrate specificity. Nat Commun. 2024;15(1):10165. doi: 10.1038/s41467-024-54500-x
77. Du M, Li N, Li T, et al. Chimeras co-targeting antigens and FcγRIIb trigger degradation of extracellular soluble proteins and pathological aggregates. Nat Commun. 2026;17(1):514. doi: 10.1038/s41467-025-67207-4

**• Characterises extracellular protein-degrading chimeras with nanoDSF and tests simultaneous antigen and FcγRIIb engagement by sequential surface plasmon resonance.**

78. Békés M, Langley DR, Crews CM. PROTAC targeted protein degraders: the past is prologue. Nat Rev Drug Discov. 2022;21(3):181–200. doi: 10.1038/s41573-021-00371-6
79. Hopkins AL, Groom CR. The druggable genome. Nat Rev Drug Discov. 2002;1(9):727–730. doi: 10.1038/nrd892
80. Frost A, O'Connor S, Ciulli A. Allosteric PROTACs: expanding the horizon of targeted protein degradation. J Am Chem Soc. 2026;148(3):2823–2837. doi: 10.1021/jacs.5c14840
81. Roy MJ, Winkler S, Hughes SJ, et al. SPR-measured dissociation kinetics of PROTAC ternary complexes influence target degradation rate. ACS Chem Biol. 2019;14(3):361–368. doi: 10.1021/acschembio.9b00092
82. Wurz RP, Rui H, Dellamaggiore K, et al. Affinity and cooperativity modulate ternary complex formation to drive targeted protein degradation. Nat Commun. 2023;14(1):4177. doi: 10.1038/s41467-023-39904-5
83. Zorba A, Nguyen C, Xu Y, et al. Delineating the role of cooperativity in the design of potent PROTACs for BTK. Proc Natl Acad Sci U S A. 2018;115(31):E7285–E7292. doi: 10.1073/pnas.1803662115
84. Riching KM, Mahan S, Corona CR, et al. Quantitative live-cell kinetic degradation and mechanistic profiling of PROTAC mode of action. ACS Chem Biol. 2018;13(9):2758–2770. doi: 10.1021/acschembio.8b00692
85. Keuler T, Ferber D, Engelhardt J, et al. Degrading the key component of the inflammasome: development of an NLRP3 PROTAC. Chem Commun (Camb). 2025;61(14):3001–3004. doi: 10.1039/D4CC06321J
86. Mühle J, Alenfelder J, Rodrigues MJ, et al. Cyclic peptide inhibitors function as molecular glues to stabilize Gq/11 heterotrimers. Proc Natl Acad Sci U S A. 2025;122(19):e2418398122. doi: 10.1073/pnas.2418398122
87. Beveridge R, Kessler D, Rumpel K, et al. Native mass spectrometry can effectively predict PROTAC efficacy. ACS Cent Sci. 2020;6(7):1223–1230. doi: 10.1021/acscentsci.0c00049
88. Hentze MW, Castello A, Schwarzl T, et al. A brave New World of RNA-binding proteins. Nat Rev Mol Cell Biol. 2018;19(5):327–341. doi: 10.1038/nrm.2017.130

89. Byun WG, Lim D, Park SB. Small-molecule modulators of protein-RNA interactions. Curr Opin Chem Biol. 2022;68:102149. doi: 10.1016/j.cbpa.2022.102149
90. Li Q, Kang C. Targeting RNA-binding proteins with small molecules: perspectives, pitfalls and bifunctional molecules. FEBS Lett. 2023;597(16):2031–2047. doi: 10.1002/1873-3468.14710
91. Wu P. Inhibition of RNA-binding proteins with small molecules. Nat Rev Chem. 2020;4(9):441–458. doi: 10.1038/s41570-020-0201-4
92. Sikorska J, Hou Y, Chiurazzi P, et al. Characterization of RNA driven structural changes in full length RIG-I leading to its agonism or antagonism. Nucleic Acids Res. 2023;51(17):9356–9368. doi: 10.1093/nar/gkad606
93. Qiu X, Kemker C, Goebel GL, et al. Phenylpyrazoles as inhibitors of the m6A RNA-binding protein YTHDF2. JACS Au. 2025;5(2):618–630. doi: 10.1021/jacsau.4c00754
94. Geng J, Chrabaszczewska M, Kurpiejewski K, et al. Cap-related modifications of RNA regulate binding to IFIT proteins. RNA. 2024;30(10):1292–1305. doi: 10.1261/rna.080011.124
95. Larsson JNK, Kumar R, Buratti FA, et al. Heat shock protein 10 as a chaperone modulating α-synuclein amyloid fibril formation. Protein Sci. 2026;35(2):e70452. doi: 10.1002/pro.70452
96. Grummitt CG, Townsley FM, Johnson CM, et al. Structural consequences of nucleophosmin mutations in acute myeloid leukemia. J Biol Chem. 2008;283(34):23326–23332. doi: 10.1074/jbc.M801706200
97. Abramson J, Adler J, Dunger J, et al. Accurate structure prediction of biomolecular interactions with AlphaFold 3. Nature. 2024;630(8016):493–500. doi: 10.1038/s41586-024-07487-w
98. Tuttle MD, Comellas G, Nieuwkoop AJ, et al. Solid-state NMR structure of a pathogenic fibril of full-length human α-synuclein. Nat Struct Mol Biol. 2016;23(5):409–415. doi: 10.1038/nsmb.3194
99. Bertoni D, Tsenkov M, Magana P, et al. AlphaFold protein structure database 2025: a redesigned interface and updated structural coverage. Nucleic Acids Res. 2026;54(D1):D358–D362. doi: 10.1093/nar/gkaf1226
100. Gallo A, Lo Sterzo C, Mori M, et al. Structure of nucleophosmin DNA-binding domain and analysis of its complex with a G-quadruplex sequence from the c-MYC promoter. J Biol Chem. 2012;287(32):26539–26548. doi: 10.1074/jbc.M112.371013
101. Urbaneja MA, Skjærven L, Aubi O, et al. Conformational stabilization as a strategy to prevent nucleophosmin mislocalization in leukemia. Sci Rep. 2017;7(1):13959. doi: 10.1038/s41598-017-14497-4
102. He D, Zhu Y, Zhong J, et al. Study of the blood-brain barrier-penetrating kras G12C inhibitor JMKX1899 in kras G12C-mutated NSCLC with brain metastases. J Natl Cancer Cent. 2026;6(3):286–296. doi: 10.1016/j.jncc.2025.11.003
103. Dusa A, Kaylor J, Edridge S, et al. Characterization of oligomers during alpha-synuclein aggregation using intrinsic tryptophan fluorescence. Biochemistry. 2006;45(8):2752–2760. doi: 10.1021/bi051426z
104. Malhotra P, Udgaonkar JB. How cooperative are protein folding and unfolding transitions? Protein Sci. 2016;25(11):1924–1941. doi: 10.1002/pro.3015
105. Alali S, Riazi G, Ashrafi-Kooshk MR, et al. Cannabidiol inhibits tau aggregation in vitro. Cells. 2021;10(12):3521. doi: 10.3390/cells10123521
106. Baggett DW, Nath A. Structure-activity relationships of novel tau ligands: passive fibril binders and active aggregation inhibitors. ACS Chem Biol. 2022;17(3):701–708. doi: 10.1021/acschembio.2c00012
107. Duy C, Fitter J. How aggregation and conformational scrambling of unfolded states govern fluorescence emission spectra. Biophys J. 2006;90(10):3704–3711. doi: 10.1529/biophysj.105.078980
• **Shows how aggregation and conformational changes in unfolded proteins alter intrinsic-fluorescence emission spectra.**
108. Augustijn D, Mahapatra S, Streicher W, et al. Novel non-linear curve fitting to resolve protein unfolding transitions in intrinsic fluorescence differential scanning fluorimetry. Eur J Pharm Biopharm. 2019;142:506–517. doi: 10.1016/j.ejpb.2019.06.001
109. Wu T, Gale-Day ZJ, Gestwicki JE. Dsfworld: a flexible and precise tool to analyze differential scanning fluorimetry data. Protein Sci. 2024;33(6):e5022. doi: 10.1002/pro.5022
110. Burastero O, Niebling S, Defelipe LA, et al. eSPC: an online data-analysis platform for molecular biophysics. Acta Crystallogr D Struct Biol. 2021;77(Pt 10):1241–1250. doi: 10.1107/S2059798321008998
111. Niebling S, Burastero O, Bürgi J, et al. FoldAffinity: binding affinities from nDSF experiments. Sci Rep. 2021;11(1):9572. doi: 10.1038/s41598-021-88985-z
112. Martin-Malpartida P, Torner C, Martinez A, et al. TPPU_DSF: a web application to calculate thermodynamic parameters using DSF data. J Mol Biol. 2024;436(17):168519. doi: 10.1016/j.jmb.2024.168519
113. Nikam R, Kulandaisamy A, Harini K, et al. ProThermDB: thermodynamic database for proteins and mutants revisited after 15 years. Nucleic Acids Res. 2021;49(D1):D420–D424. doi: 10.1093/nar/gkaa1035
114. Cohrs M, Davy A, Van Ackere M, et al. Intrinsic differential scanning fluorimetry for protein stability assessment in microwell plates. Mol Pharm. 2025;22(3):1697–1706. doi: 10.1021/acs.molpharmaceut.4c01496
•• **Demonstrates intrinsic-fluorescence thermal profiling in 384-well plates and benchmarks it against calorimetry and circular dichroism.**
115. Tsvetkov PO, Eyraud R, Ayache S, et al. An AI-powered blood test to detect cancer using nanoDSF. Cancers (Basel). 2021;13(6):1294. doi: 10.3390/cancers13061294
116. Kroupova A, Spiteri VA, Rutter ZJ, et al. Design of a Cereblon construct for crystallographic and biophysical studies of protein degraders. Nat Commun. 2024;15(1):8885. doi: 10.1038/s41467-024-52871-9
• **Describes the design and biophysical assessment of a cereblon construct suited to structural and binding studies of protein degraders.**